ARPA ORDER NUMBER-356
PROJECT CODE NUMBER-5730

RESEARCH ON PROPERTIES OF LASER DEVICES*

FIRST
TECHNICAL SUMMARY REPORT
AF 49 (638)-1535
15 NOVEMBER 1964 THROUGH 15 MAY 1965

SUBMITTED BY:

TRG INCORPORATED
A SUBSIDIARY OF CONTROL DATA CORPORATION
ROUTE 110
MELVILLE, NEW YORK

*This research is a part of Project DEFENDER, sponsored by Advanced Research Projects Agency, Department of Defense and technically monitored by the Air Force Office of Scientific Research, under Contract AF 49(638)-1535.

ARPA Order Number - 356
Project Code Number - 5730

TRG-034-TR-1

RESEARCH ON PROPERTIES OF LASER DEVICES*

FIRST
TECHNICAL SUMMARY REPORT
AF 49(638)-1535

15 November 1964 through 15 May 1965

Submitted by:

TRG Incorporated
A Subsidiary of
Control Data Corporation
Route 110
Melville, New York

Edited by: N. Solimene
N. Solimene

Approved by: Gordon Gould
G. Gould
Project Leader

R. T. Daly
R. T. Daly
Department Head

*This research is a part of Project DEFENDER, sponsored by Advanced Research Projects Agency, Department of Defense and technically monitored by the Air Force Office of Scientific Research, under Contract AF 49(638)-1535.

AUTHORS

Portions of this report were written by:

S. Jarrett
M. Piltch
C. Roth
B. Senitzky
S. D. Sims
A. Stein
W. Walter

TABLE OF CONTENTS

LIST OF ILLUSTRATIONS

ABSTRACT

Experimental work on gaseous and solid-state laser development is reported. The high temperature Mn collision laser tests indicated that insufficient gain was achieved to obtain oscillation with present apparatus. Experiments testing La and Y as collision laser media were concluded after demonstrating that higher discharge currents and higher operating temperatures than presently available were required. The possibility that photodissociation of TlBr in the presence of a quenching gas could lead to a population inversion was experimentally investigated. Mach-Zehnder interferograms of the transient optical path distortions introduced by optical pumping of ruby were obtained. An R_1 ruby laser pumped by an R_2 ruby laser experiment was designed and the construction of the apparatus initiated.

1. INTRODUCTION AND SUMMARY

The goal of this program has been the development of lasers with higher brightness, power and efficiency than presently available. The research tasks have been divided into the two major parts consisting of research on the properties of gaseous lasers on the one hand and solid-state lasers on the other.

The work performed in the area of gaseous laser development is a continuation of work initiated during the previous contract: AF 49(638)-673. Experiments have been performed on two new types of gas lasers. One of these, known as the collision laser, is based on the utilization of collisional relaxation. The other depends on creation of population inversions by the photodissociation of molecules.

A number of elements were considered as candidates for collision laser media. Those felt to be the most promising turned out to be elements which require high temperatures in order to obtain adequate vapor pressures. As a result considerable time and effort has been devoted to successive redesign and reconstruction of experimental apparatus. After construction of one apparatus capable of operation up to 1400°C and another of operation up to 2000°C, experiments were performed to test the concept of the collision laser. The lower temperature apparatus was employed in the investigation of manganese and various noble gas mixtures under a variety of discharge conditions. The higher temperature apparatus was used to similarly investigate lanthanum and yttrium. To date neither effort has led to laser oscillation. In the case of manganese it is believed that appropriate conditions for population inversion have been achieved, but that the transition probability for the proposed laser transition is so small that oscillation would not be possible in the present apparatus. In the case of lanthanum, the thermal ionization which sets in at relatively low temperatures ($\sim$1600°C) has prevented the attainment of collision laser discharge conditions. With yttrium, it is believed that the electron excitation rates are insufficient compared to collisional

and radiative relaxation to permit the attainment of population inversions. Work on the rare-earth collision laser has therefore been terminated. Additional investigations are in progress to verify the tentative conclusion concerning the manganese system.

The work on the photodissociative pumping mechanism has been mainly concerned with the measurement of absorption and quenching cross-sections. These basic parameters have been investigated in order to determine the extent by which the creation of population inversion has been missed. It was concluded that with TlBr and various quenching gases, population inversions could not be maintained. Similar investigations for CsCl are planned.

The solid-state laser investigations have been concerned with the elucidation of the reasons for the poor radiance which is usually exhibited by solids. Among the proposed causes are the thermo-optical effects due to the presence of thermal gradients. The thermal gradients are the result of pump light absorption. A Mach-Zehnder interoferometer was used to investigate the time development of the optical properties both during and after a pump pulse. A significant result of this work is the apparent reproducibility of the interferograms from shot-to-shot. A second line of investigation has been concerned with the avoidance of the thermo-optical effects by decreasing to a minimum the pump light which must be absorbed. Thus an R_2 ruby laser may be used to pump an R_1 ruby laser with very little heat deposition expected. Consequently the radiance of the R_1 laser should be improved to whatever extent its performance had been limited by thermal effects. The design and construction of the necessary apparatus for a laser pumping laser experiment has been undertaken.

2. MANGANESE COLLISION LASER

The manganese-noble gas system was investigated for the purpose of demonstrating the collision laser principle. The principle of operation is described in detail in the paper by Gould*.

Experimental Apparatus

Several types of experimental apparatus were constructed which were capable of producing and enclosing manganese vapor (at 1400°C) under vacuum conditions in an optical cavity. The first two designs were constructed, tested and rejected as described in a previous report**. The Mark III apparatus also described in this reference suffered from the difficulty of replenishing the active material supply once it had migrated out of the heated zone. On the basis of diffusion calculations one should have expected one 10 g charge of Mn to have provided an experimental lifetime of several hundred hours. In fact, the lifetime was of the order of 10 hours which pointed to other means of mass transfer, such as convection. In view of these circumstances, an apparatus was designed and constructed using brazed alumina to Kovar seals, demountable O-ring sealed electrode-window assemblies and replaceable alumina liners. This scheme facilitates easy loading and replenishing of the active material.

Mullite, magnesia, alumina, beryllia and thoria were considered as possible laser tube construction materials. Alumina was chosen because it has excellent vacuum properties at high temperatures, it is mechanically strong, can be bonded to metal and is available in long lengths. The type of alumina chosen was the recrystallized type of 99.5% purity which is used in production of ceramic-metal vacuum tubes. The tube construction gravitated naturally to the ceramic-metal method. Measurements show that in the range of temperatures 100-1000°C the coefficient of thermal expansion of alumina closely matches that of Kovar alloy. This consideration and the ease of brazing and welding Kovar made it ideal for

---

* G. Gould, Appl. Opt. Suppl. 2, 59 (1965).

** TRG-134-QTR-9 on Contract AF 49 (638)-673.

use in seals. Several processes were developed for the actual bonding of alumina to Kovar. They all involve two steps: (1) applying a closely adhesive or chemically bonded metal layer on the alumina ceramic and (2) brazing or soldering the required part to the metallized region of the ceramic. It has been experimentally determined* that colloidal mixtures of molybdenum and manganese of 1-5 micron particle size when applied to alumina along with a liquid binder and fired at about 1350°C produced a strongly bonded metallic layer which penetrates the order of 0.1 mm into the ceramic. If this layer is electroplated with nickel or copper the ceramic part can then be brazed to the similarly plated Kovar part. Usually the alumina is placed on the inside of the Kovar part in cylindrically symmetric structures to maintain it in a state of compression.

In the coaxial tube structure the outer alumina tube has a Kovar flange brazed to each end. The joining Kovar tube has a 0.010 wall thickness for flexibility and surrounds the alumina. The braze was done with B-T material, a silver-copper eutectic alloy with a melting point of 780°C. All metallizing and brazing was done in molybdenum wound electric ovens using dissociated ammonia atmospheres. Very careful attention was paid to heating and cooling rates to avoid breakage by thermally shocking the alumina. Rates of 200°C per hour were followed because of the poor thermal conductivity of alumina and the relatively large wall thickness of the tubes.

The actual apparatus used (see Figure 1) has a coaxial structure with an outer alumina oven tube of 1 inch o.d. x 3/4 inch i.d. x 36 inches long. The Kovar flanges brazed to its ends form vacuum tight mechanically strong supports for the electrode-window assemblies that bolt to them. One of the flanges has a vacuum pumping lead brazed to it for connection to the pumps and gas handling manifold. The inner tube is 15 mm o.d. x 10 mm i.d. x 36 inches long. It is of the same material as the outer tube: Morganite

*Handbook of Electron Tube and Vacuum Techniques, F. Rosebury, (Addison Wesley Co., Inc., Reading Mass., 1965) pp. 68-73.

"triangle RR" 99.5% pure alumina. The tube and its contents are heated by a ribbon heater of 60% platinum, 40% rhodium alloy, 0.005 inch x 0.060 inch x 50 feet wound around the 1 inch tube and bonded to its surface with "alundum" RA 1139 refractory cement. The tube is mounted in a heat insulating assembly which consists of a 14 inch o.d. x 8 inch i.d. x 36 inches long asbestos pipe insulator, a layer of alumina firebrick and a primary insulator of alumina grain. The grain is effective in changing the primary means of heat loss from radiation which increases as the fourth power of temperature to conduction which increases linearly with temperature.

The charge of material to be investigated is placed within the alumina liner which is inserted into the alumina oven assembly. The flanged window-electrode assemblies are bolted on and the tube evacuated. While preliminary heating is taking place the vacuum pump remains connected for outgassing purposes until the temperature is high enough to raise the vapor pressure of the active material to $\sim 10^{-6}$ Torr. At this point, a sufficient pressure of helium (about 2 Torr) is added to prevent rapid diffusion of the active material to the cool window region. Heating then proceeds until the operating vapor pressure is reached and a sufficient pressure of helium is added to conform to the desired experimental conditions.

The electrical excitation is applied by means of flashlamp electrodes which are large tungsten slugs sealed into quartz jackets. For long pulse or dc operation a thermionic cathode is used (Figure 2). A pure tungsten filament is used to avoid the contamination effects seen with thoriated tungsten or oxide coated cathodes. All electrodes are forced air cooled, especially the thermionic cathode which requires 300 watts heater power for 10A thermionic emission.

Radiation exits from the excited active material through either BaF_2 or quartz windows. Since the windows remain under cool ambient conditions they are bonded to the electrode assembly with epoxy vacuum cement. In order to protect the inner surface of the

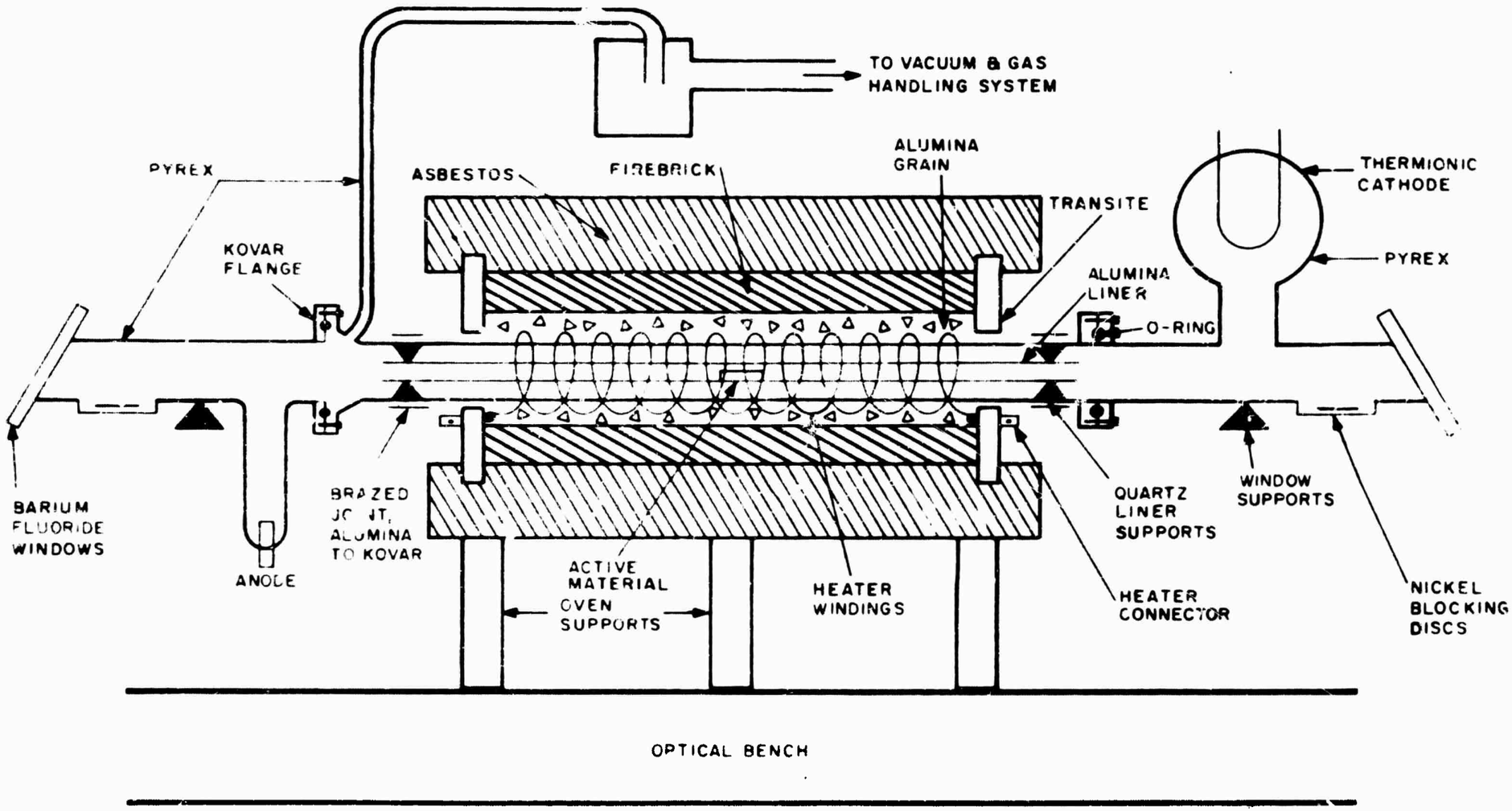

FIGURE 1. COLLISION LASER APPARATUS

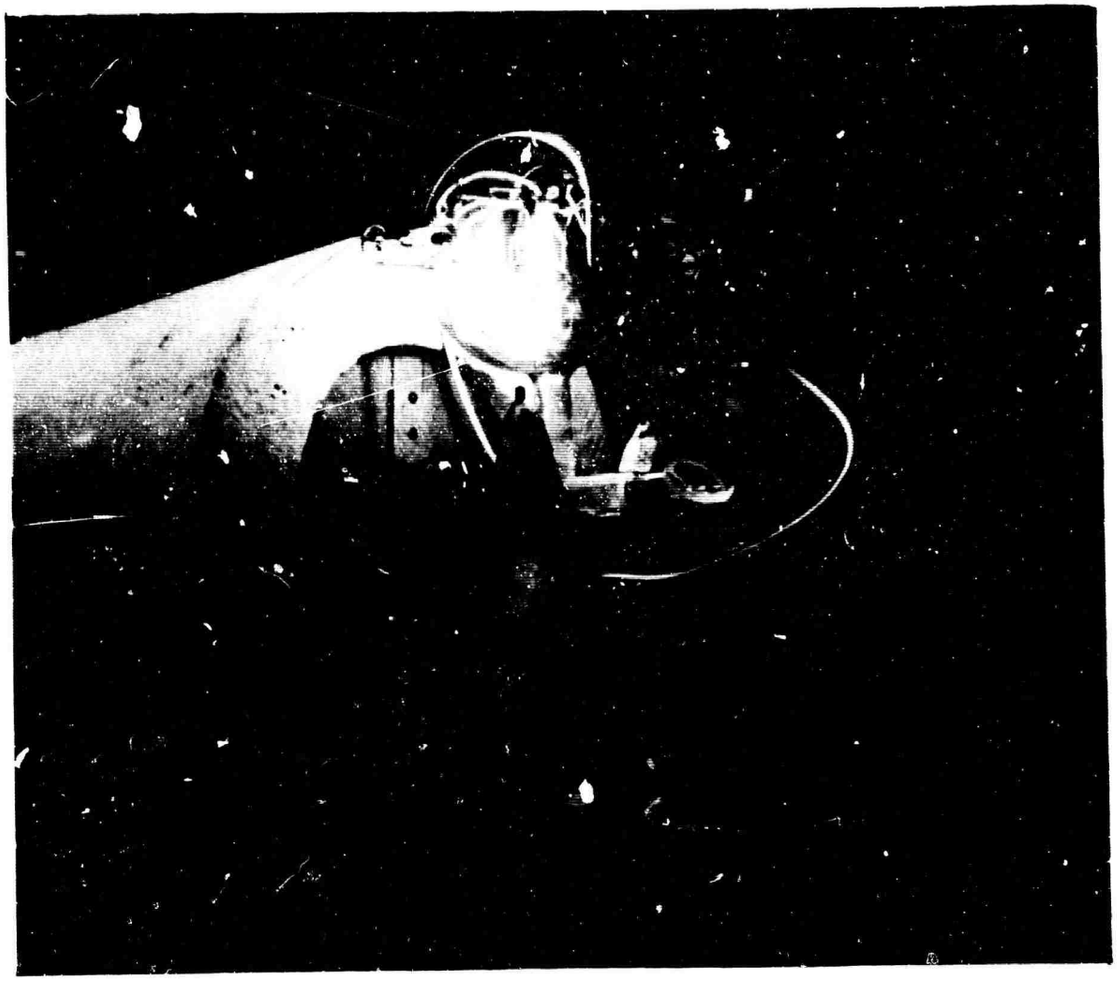

FIGURE 2. THERMIONIC CATHODE AS USED ON ALUMINA LASER TUBE

windows from deposits of the active material which might diffuse to them, small nickel discs are placed in a recessed area near the window. While measurements are not being made the discs are raised with the aid of a small magnet and effectively block any migration to the window.

Several different power supplies were used in exciting the metallic vapors. Initially, a dc source was used; it was sine wave modulated and capable of 5000 Vrms and 2 A average current. The sine wave modulation served two purposes: (1) to modulate the light output for phase sensitive detection of spontaneous emission and (2) to subject the atomic system to varying current densities, since the optimum electron density for laser action was not known. This same supply was capable of being modulated with 50% duty cycle square waves of 4 A peak current.

The next power supply was a pulsed device using hard tubes as the modulators. The pulse width was variable from 0.2 msec to 1.8 msec, a pulse repetition rate from 2 cps to 500 cps with the capability of 5000 V at peak currents of 12 A. This system supplied reference voltages and a stable repetition rate for use with phase sensitive detection equipment.

Experimental Results

Upon completion of the ceramic-metal flanged system an attempt was made to observe the manganese spectral lines favorable for CW oscillation as a collision laser. These were in the 2.0μ to 2.2μ and 2.6μ to 2.7μ ranges corresponding to a^4D to z^8P^o and $^4P^o$ to a^4P transitions respectively. A Perkin-Elmer model 98 g monochrometer with an Eastman Kodak N type PbS cell, and a Sanborn phase sensitive detector were used to detect the signal. A wide range of current densities, Mn pressures and discharge carrier gas pressures were tried but none of the expected lines were seen in spontaneous emission although numerous other manganese infrared lines were observed. At this point, it was decided to determine if the upper and lower laser levels were truly in Boltzmann equilibrium at or near the electron temperature. Apparatus was set up to observe spontaneous emission from energy levels near the expected laser level.

Convenient lines were the strong Mn resonance lines originating from the z^8P^o level centered at 18500 cm^{-1} and those originating from the z^6P^o group at 24800 cm^{-1}. Lines from these levels appeared at 5395Å and 5433Å and 4030Å to 4034Å respectively. It was possible to saturate the population density in these levels as indicated by the leveling off of the line intensity as a function of excitation current density in the neighborhood of 3 to 10 A cm^2. This result demonstrated that population equilibrium at or near the electron temperature had been established at least up to an energy of 25000 cm^{-1}. Therefore the failure to observe spontaneous emission at the proposed laser transitions was attributed to A coefficients of less than expected magnitudes. An absolute power calibration of the detection system was made to provide an upper limit on the A value of the laser transitions, and consequently, a maximum figure for the laser gain. Careful calibration with an Eppley-NBS standard lamp showed that intensities corresponding to A coefficients of 0.25 sec^{-1} at wavelengths of about 2.. were detectable. This upper limit on the A coefficient indicated that the laser transition gain had to be less than 0.8% per meter. Had the gain been twice this amount, oscillation would have been observed.

Future Work

An optimization of the optical system is planned. Reflectors of the highest possible reflectivity to allow even very weak transitions to oscillate will be obtained. A barium fluoride pick-off plate will be inserted in the optical cavity to extract radiation. Since the basic apparatus has proved very reliable and experimentally convenient there are no plans to modify it. A new power supply is being constructed to provide excitation current pulses of extremely fast rise time. It will utilize a capacitor or transmission line discharging into the laser tube through an air spark gap.

3. RARE EARTH COLLISION LASER

The purpose of this experiment is to investigate the rare earth elements lanthanum and yttrium for suitability as collision laser media. Both La and Y exhibit the necessary level structure for a collision laser, i.e., two groups of levels separated by an energy large compared to thermal energy and the levels within these groups separated by energies approximating thermal energy. For a collision laser to work, the two groups of levels must have a population ratio determined by a high temperature, (the electron temperature) while the population within a group must be distributed according to a low temperature (the gas kinetic temperature). The work described in this section was intended to demonstrate that the former condition could be achieved in a rare earth discharge. The results were negative and a decision to suspend work on the rare earths was made. This decision was based upon the experimental difficulties in achieving a distribution of populations between the groups of levels according to the electron temperature. No fundamental inability to do this was demonstrated.

Rare Earth Laser Tube

The physical properties of La and Y put severe requirements on an apparatus one might build to produce a discharge in their vapors. These properties are: (1) Vaporization Temperature*: La requires a temperature of 1950°C to achieve a vapor pressure of 0.1 Torr; Y similarly to achieve a vapor pressure of 0.1 Torr, requires 1820°C. (2) Chemical Reactivity*: La and Y are reduced by oxide crucibles and metal crucibles must be used. These two limitations led to a design in which a resistance heated tantalum (Ta) seamless tube was used to vaporize the rare earths. This design meant that a geometry other than the usual longitudinal discharge, parallel to the tube axis, had to be used, since the metal walls

*R.J. Ackermann and E.G. Rauh, J. Chem. Phys. 36, 448 (1962)
C.E. Habermann and A.H. Daane, J. Chem. Phys. 41, 2818 (1964).

are unable to support the voltage drop necessary to maintain the discharge. Thus, a transverse discharge was used, with the current flowing from a hot tungsten ribbon filament suspended along the tube axis radially to the Ta cylinder. Figure 3 shows the details of the laser tube with provision for this transverse discharge.

After construction and operation of the laser tube, two unavoidable problems became apparent. First, Ta recrystallizes in a vacuum and loses mechanical strength at the temperatures of operation (up to 1800°C). This caused failure after ~100 hours of operation. Second, this type of transverse discharge limited the current density to 1.5 A/cm^2 over the approximately 15 cm hot zone and in a region 2 mm from the tungsten ribbon. To achieve higher current densities, the tube was converted to longitudinal operation through use of two thoria tubes placed into the Ta tube and set into boron nitride end pieces held between the copper cathode block and the end flanges. The rare earths do react with the thoria as mentioned before. To prevent rapid destruction of the thoria, the bulk rare earth was kept in a short (4 inch) section of Ta joining the two thoria tubes. Both types of discharge were used during the course of the experiments. A rare gas, either He or Ar at a pressure of 50 Torr was used to prevent rapid diffusion of the metal from the hot zone.

Experimental Results

In order that the groups of levels in La and Y come to equilibrium at the electron temperature, electron atom collisions must predominate over all other processes, collision and radiative, in the gas discharge. To test for this, one can search for saturation of fluorescence from the levels in question as the current is increased. The energy levels are shown in Figure 4. The transitions are in La the 5d 6s^2) 6p $^4F^o_{5/2}$ to 5d^2(^{3}P) 6s $^2P_{3/2}$ at 2.555μ and in Y the 4d 5s^2 D)5p $^4F^o_{5/2}$ to 4d^2(^{3}F)5s $^4F_{7/2}$ at 2.502μ and the 4d 5s(^{3}D)5p $^4F^o_{3/2}$ to 4d^2(^{3}F)5s $^4F_{5/2}$ at 2.583μ. These transitions were observed in the discharge using a Jarrell-Ash Model 82-000 0.5 Ebert monochromator and an n-type PbS photoconductor. The attempt to observe saturation as a function of discharge current constituted the bulk of the experimental work.

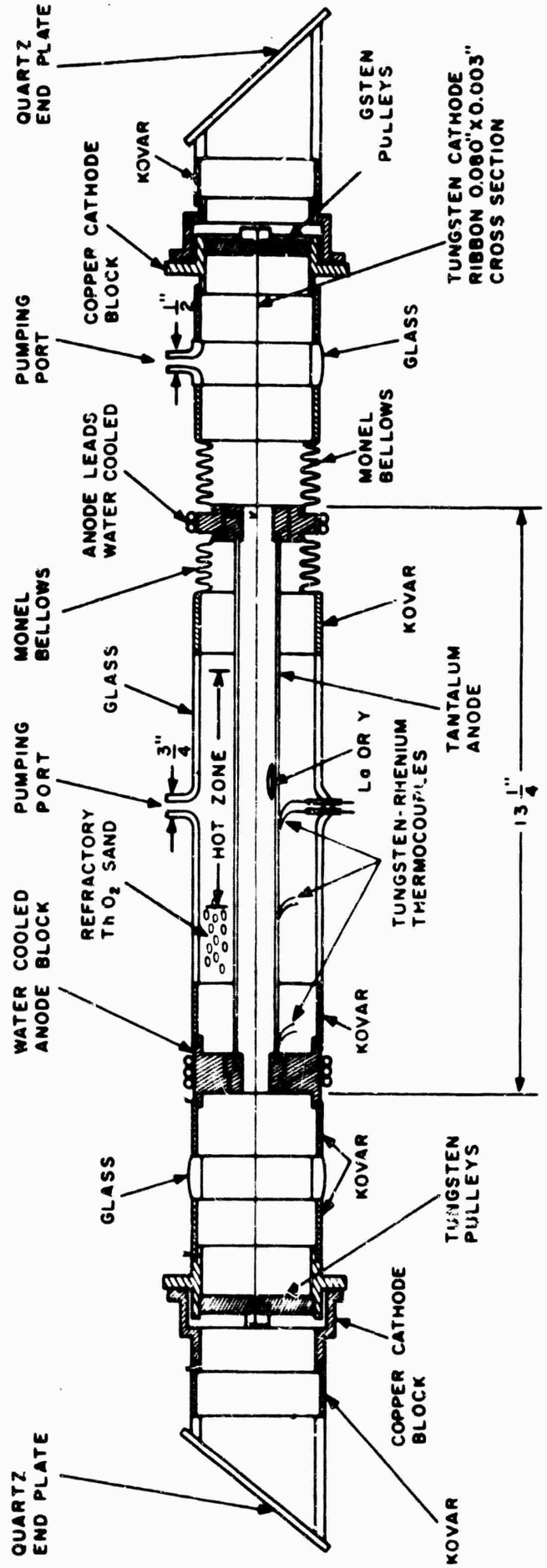

FIGURE 3. RARE EARTH COLLISION LASER TUBE WITH PROVISION FOR TRANSVERSE DISCHARGE

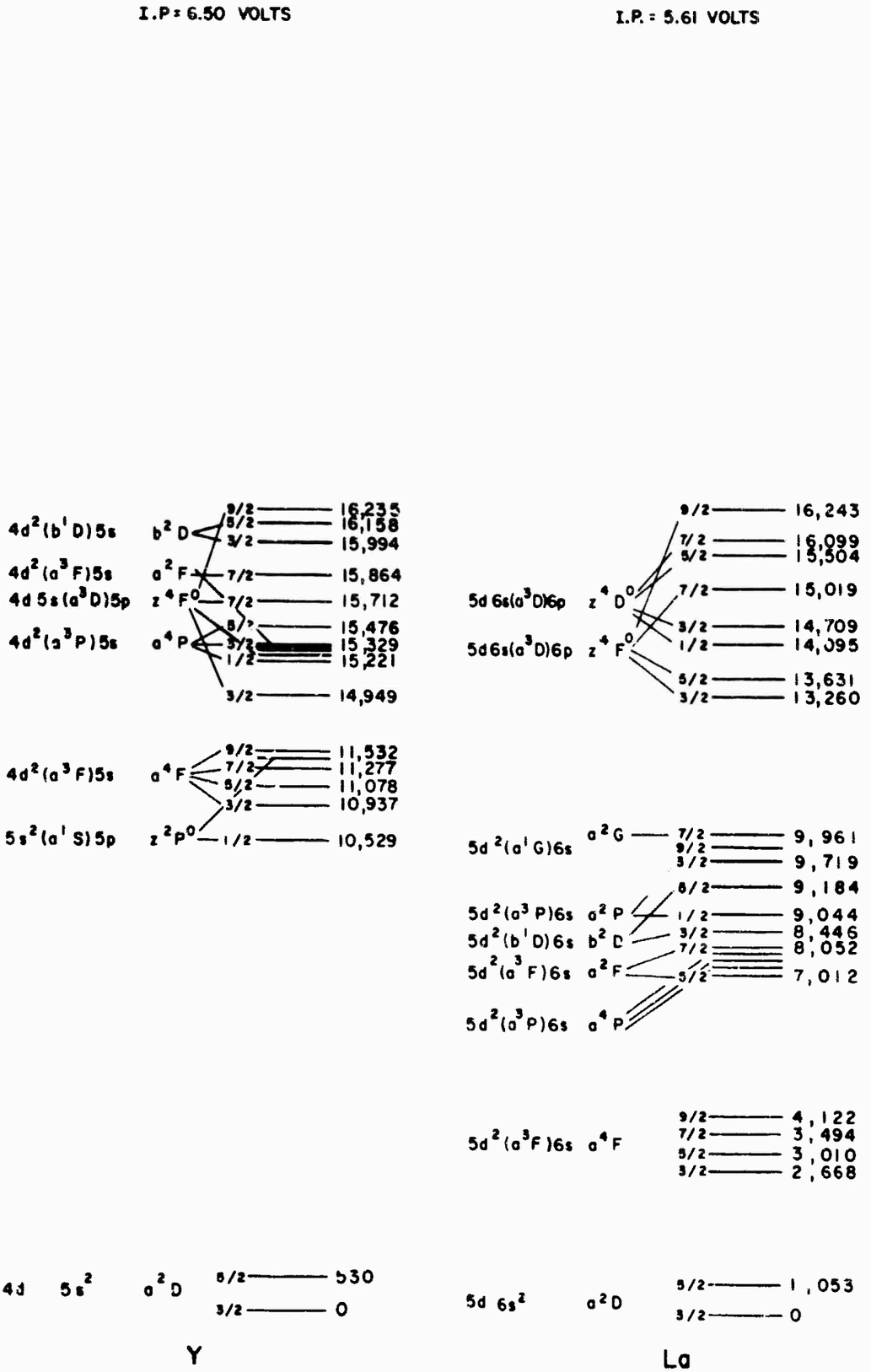

FIGURE 4. ENERGY LEVELS OF Y AND La

Lanthanum was placed at the center of the cylindrical Ta tube. The line spectrum was photoelectrically recorded as the difference between the emission intensity with the discharge current off and on. This eliminated the detection of unwanted thermal background radiation. The temperature of the evacuated tube was raised to 1000°C prior to filling with 50 Torr He. At temperatures less than 1400°C, only an He spectrum was recorded. As the temperature is further increased, an La and LaO spectrum is observed. At temperatures above 1800°C (maximum temperature reached was 1870°C), all spectral lines disappeared. This effect is due to thermal ionization of La (I.P. = 5.6 eV). The effect of this thermal ionization is to decrease the voltage across the discharge and thus lower the electron temperature. An upper limit of the working temperature for La is thus established. At 1800°C, the vapor pressure is 20 mTorr. Thus, one finds the effect of turning the discharge on and off becomes less and less as 1800°C is approached. An increase and an eventual decrease in spontaneous emission is observed in the proposed laser transition as the temperature is increased. An attempt to observe saturation was made on the 2.555μ line at 1650°C (P_{La} = 3 mTorr) but no saturation was observed with current densities of up to 1.5 A/cm^2. A search for oscillation produced netative results.

Yttrium demonstrated its superiority over La in the next series of experiments. First no spectral evidence of any yttrium oxide was found. Second, the Y spectrum continued to increase monotonically with temperature to 1800°C, i.e., there was no apparent effect of thermal ionization. This is due to the higher ionization potential, 6.5 eV, of Y. The lines at 2.520μ and 2.583μ were observed and their current dependence was studied. Using the transverse discharge as in the La experiment, at a pressure of 40 mTorr of Y and currents up to 1.5 A/cm^2, no indication of current saturation of fluorescence was observed on either line. At this point, the Ta laser tube was adapted for a longitudinal discharge so that current densities could be increased to 20 A/cm^2. Still no evidence of saturation was observed. Not withstanding the absence of saturation, a search for oscillations was made but the results were negative.

The inability to saturate the Y transitions demonstrate that other processes are proceeding at a more rapid rate in the discharge than electron-atom inelastic collisions. One immediately suspects spontaneous emission from the upper levels. Recent measurements* in La and Y show that A values for spontaneous emission from the upper laser levels to the ground state are 3×10^5 sec^{-1}, 1.2×10^5 sec^{-1} and, 4×10^4 sec^{-1}. These rates must be exceeded by the electron atom inelastic collision rates unless there is radiation trapping. The process of radiation trapping cannot be of much help since diffusion of excited atoms to the laser tube walls and subsequent collisional de-excitation could proceed as rapidly as 10^3 sec^{-1}. Therefore, higher currents and some increase in tube operating temperatures are required for saturation. Neither are possible with the present apparatus.

Future Work

No further work on the rare earths is contemplated.

*C.H. Corliss and W.R. Bozman, Experimental Transition Probabilities of Spectral Lines of Seventy Elements, (U.S. Government Printing Office, Washington, D.C., 1962) N.B.S. Monograph 53.

4. PHOTODISSOCIATION LASERS

The goal of the work on molecular photodissociation is the development of an efficient, high power gas laser. The advantage of a molecular laser medium lies in the broad molecular photodissociative absorption band ($\sim$3500 cm^{-1}) which is 10^5 times broader than an atomic absorption line. This will permit an increase by the same factor of pumping light power coupled into a molecular gas-laser medium over the coupling possible into an atomic laser medium. When a suitable molecule can be paired with a lamp whose output is confined largely to the 3500-cm^{-1} photodissociative absorption-bandwidth of the molecule, a continuous gas laser with watts of output in the visible will be possible.

The 1850Å mercury line has been selected as the optical pumping source. Although far from optimum, this source appears to be the best available at the present time. Two systems have been chosen for investigation*, thallium bromide and the cesium halides. These are the most promising of the molecules presently known to be photodissociated by the 1850Å line.

TℓBr Photodissociative Laser

A TℓBr photodissociation laser is expected to operate as follows:

$$T\ell Br + h\nu\ (1850\text{Å}) \rightarrow T\ell^*(7^2S_{1/2}) + Br \qquad (1)\ \text{excitation}$$

$$T\ell^*(7^2S_{1/2}) \rightarrow T\ell^m(6^2P_{3/2}) + h\nu(5350\text{Å}) \qquad (2)\ \text{laser}$$

$$T\ell^m(6^2P_{3/2}) + X \rightarrow T\ell + X^* \qquad (3)\ \text{relaxation}$$

$$T\ell + Br + Y \rightarrow T\ell Br + Y^* \qquad (4)\ \text{recombination}$$

A rate equation calculation has been made to determine the optimum operating temperature and maximum gain expected when the population of the lower laser level is neglected. This calculation indicated that a gain of 19%/m would be expected when the operating temperature

*W.T. Walter & S.M. Jarrett, Appl. Opt. Suppl. 2, 201 (1965)

of TlBr was 660°C. Absolute intensity measurements of the 5350Å Tl fluorescence have indicated a maximum upper level population of 40% of the 9 x ^{7} cm^{-3} expected. This was achieved when the TlBr temperature was 500°C. The Hg lamp was pulsed on for 330 μsec periods at a 100 cps rate. This excitation rate may just be sufficient, so attention was turned to the problem of finding a gas to selectively quench the Tl metastable level (i.e., X in process (3) above).

Tl Quenching Gas

Is it possible to find a quenching gas for the metastable Tl level? Direct measurements have not been reported in Tl. Several quenching experiments*, however, have been performed in Hg where the character of the first three levels is the same as in Tl, although the relative spacing between the Hg levels is inverted with respect to the situation in Tl. In other words, the second level, which is metastable in both, is much closer to the ground level in Tl than in Hg (see Figure 5). The earlier experiments* indicated that some gases preferentially quench the upper Hg level to the ground level (hydrogen, for example) while others (e.g., N_2 and CO) preferentially quench the upper Hg level to the metastable $^{3}P_{o}$ level. This demonstrates that collisional quenching can be used to relax an excited atomic level to a level which is not optically connected to the first in preference to an optically connected level and at a rate more rapid than the allowed spontaneous-emission rate. The situation in Tl is similar except that the allowed transition is inverted, filling instead of emptying the level to be quenched. Thus it seems reasonable to expect that a gas can be found which will selectively quench the Tl metastable level.

An additional difference exists between the situations in mercury and thallium. The spacing between the $6^{3}P_{1}$ and $6^{3}P_{o}$ levels in Hg is only 0.2 eV while the spacing between the $6^{2}P_{3/2}$

*A.C.G. Mitchell and M.W. Zemansky, Resonance Radiation and Excited Atoms (Cambridge Univ. Press, Cambridge, 1934) p. 65-66 and 223-225.

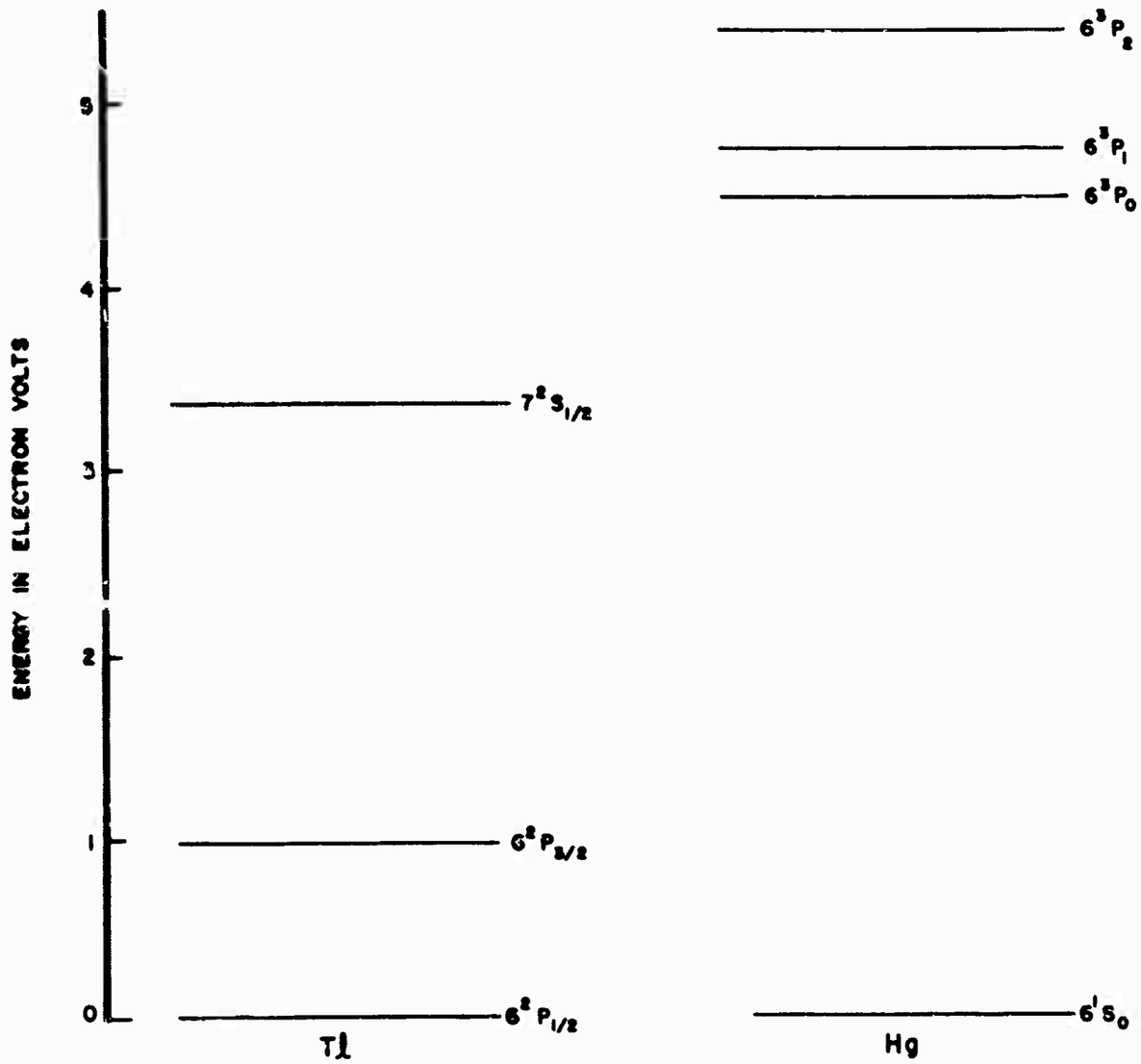

FIGURE 5. THALLIUM-MERCURY ENERGY LEVEL COMPARISON

and $6^2P_{1/2}$ levels in Tℓ is 0.97 eV. Molecules like N_2 and CO which selectively quench the Hg 6^3P_1 level to the metastable 6^3P_o have first vibrational levels 0.2 eV above their ground levels. No diatomic molecule has been found whose first vibrational level is as much as 1 eV above its ground level. Hydrogen is 0.5 eV. Therefore, the quenching cannot be accomplished by means of an energy correspondence with a molecular transition to the first vibrational level.

Quenching accomplished by a molecular transition to a vibrational level higher than the first has also been considered. A number of diatomic molecules were examined for vibrational levels close to 0.97 eV. Each molecule examined had higher vibrational levels with a closer energy correspondence with one or both of the Tℓ $7^2S_{1/2}$-$6^2P_{3/2,1/2}$ spacings than it did with the Tℓ $6^2P_{3/2}$-$6^2P_{1/2}$ spacing. Furthermore, the manner in which the transition probability varies with the change in vibrational quantum number, Δn, is involved as well as the change with energy defect, ΔE. The examination of diatomic vibrational levels indicates that it does not appear possible to select a diatomic quenching molecule on the basis of energy correspondence alone. For polyatomic molecules the situation is even more difficult; there are many more levels and less knowledge of the molecular constants. It appears that only by experimentation will the necessary quenching gas be found.

There are other conditions that the quenching gas must satisfy, and these were used to select the gases tried experimentally. These conditions are that the quenching gas must be transparent at the pumping and laser wavelengths, 1850Å and 5350Å, and probably also at 2537Å. The quenching gas must also not react with TℓBr, Tℓ, or Br. Simple molecular gases that appear to satisfy these conditions are N_2, CO and CO_2.

An atomic quenching gas is also a possibility; a possibility which because of the absence of band structure would be much less likely to absorb the pumping or laser wavelengths. Lead, iodine, and polonium are the three most promising possibilities. They have low lying levels that are within 27, 190, and 280 cm^{-1}

respectively of the 7793 cm^{-1} $^2P_{3/2}$ Tℓ level. The difficulty with lead is its low-vapor pressure. Temperatures from 1160°C up to 1420°C would be required to obtain the 10 to 100 Torr of lead vapor pressure that we believe is necessary. The present all-quartz system cannot be used. Lucalox (polycrystalline synthetic sapphire) could be used for the inner tube containing the TℓBr. An 0.5 mm thick tube would have a total transmission (in-line plus scattered) of 35% at 1850Å. The technique of fabricating the length and shape of the tube required has not yet been acquired by the manufacturer. Unfortunately iodine would not be any better. It occurs as a dimer in the vapor, and I_2 absorbs both at 1850Å and 5350Å. Temperatures in excess of those required for lead would be required to thermally dissociate I_2. Polonium is radioactive. However, it has a long-lived isotope, 103 year Po^{209}, which decays by alpha emission and could be safely handled in the amounts required. Apparently its vapor consists both of Po and Po_2*. It appears that at the pressures of Po needed (10 to 100 Torr at ~700°C to 900°C) there will be about three times as much Po_2 vapor. The absorption spectrum of Po_2 vapor is required to determine whether Po can be used as the quenching gas.

Quantitative requirements for several of the collision cross-sections of the quenching gas can be determined by applying the rate equations to the lower laser level, the $6^2P_{3/2}$ Tℓ level. The result is

$$\frac{n_u}{n_\ell} = \frac{\frac{D}{a^2} + \sigma'_{\ell g} v'_\ell n_m + \sigma_{\ell g} v_\ell n_q}{A_{u\ell} + \sigma'_{u\ell} v'_u n_m + \sigma_{u\ell} v_u n_q} \qquad (1)$$

where the subscripts u, ℓ, and g represent the upper ($7^2S_{1/2}$), lower ($6^2P_{3/2}$), and ground ($6^2P_{1/2}$)Tℓ levels and the subscripts m and q represent the molecular species (TℓBr) and the quenching gas. Symbol n represents the particle density (cm^{-3}), A_{ij} is the spontaneous radiative transition probability from level i to level j, σ_{ij} is the cross-section for the quenching of a Tℓ atom in

*D.R. Stull and G.C. Sinke, Thermodynamic Properties of the Elements, Advances in Chemistry, Series 18 (Am. Chem. Soc., Washington, D.C., 1956) p. 154.

level i to level j caused by a collision with the quenching gas, σ'_{ij} is a similar cross-section caused by a collision with the molecular TℓBr species, v_i is the square root of the sum of the squares of the mean velocity of the atom in the i^{th} level and the mean velocity of the quenching gas, v'_i is a similar rms velocity where the molecular TℓBr species has replaced the quenching gas, D is the diffusion constant, and a is the radius of the tube.

A necessary condition for a laser is that $n_u/n_\ell > 1$. This imposes the following conditions on the quenching gas. First $\sigma_{\ell g} > \sigma_{u\ell}$. A quenching gas must be found that has a higher cross-section to quench the lower $6^2P_{3/2}$ Tℓ level to the ground $6^2P_{1/2}$ level than it does to quench the upper $7^2S_{1/2}$ level to the lower $6^2P_{3/2}$ level. Quenching of the upper to the ground level will not affect the population inversion. It will only reduce the efficiency of the laser. Second, $\sigma_{\ell g} > 5 \times 10^{-17}$ cm^2. Under the best conditions $A_{u\ell}$ will predominate over the other terms in the denominator of Eq. (1), and $\sigma_{\ell g} v_\ell n_q$ will predominate in the numerator. Then $\sigma_{\ell g} > A_{u\ell}/v_\ell n_q$. For a reasonable maximum pressure of the quenching gas, 1 atmosphere, we find that the cross-section to quench the lower Tℓ level to the ground level must be greater than 5×10^{-17} cm^2. Although this is a sizeable cross-section, the quenching cross-sections that have been measured* for Tℓ have indicated that $\sigma_{u\ell} + \sigma_{ug} \sim 10^{-14}$ cm^2. As discussed above, there is no reason why some gases should not have $\sigma_{\ell g} > \sigma_{u\ell}$. The orbital angular momenta of the two levels are favorable; that is, the lower is a P state while the upper is an S state. Therefore there seems to be no fundamental reason why we should not be able to find a quenching gas to selectively quench the lower Tℓ level.

Experimental Results

The upper and lower Tℓ level densities, n_u and n_ℓ, were measured as a function of TℓBr pressure. An absolute intensity measurement of the 5350Å fluorescence gave an approximate value of n_u. The absorption of 5350Å fluorescence radiated from a first photodissociative tube into a second photodissociative tube, identical in every respect with the first, was used to determine n_ℓ.

*A.C.G. Mitchell and M.W. Zemansky, op. cit, p. 213.

This is the method of Ladenburg and Reiche*. The value of n_ℓ was used to correct the absolute intensity measurement of n_u.

For these experiments the Hg pumping lamps were operated on dc. The solid angle of the detected fluorescence was restricted so that radiation from the tube walls would not be collected. The results of these experiments are shown in Figure 6 and Figure 7. The experimental curve in Figure 7 does have the TℓBr pressure (n_m) dependence indicated by Eq. (1) ($n_q = 0$ here). The asymptotic value of n_u/n_ℓ at high pressures, $\sigma'_{\ell g}\bar{v}_\ell/\sigma'_{u\ell}\bar{v}_u$, is 5×10^{-3}. Since $\bar{v}_\ell/\bar{v}_u = 0.8$, it follows that $\sigma'_{\ell g}/\sigma'_{u\ell} \sim 10^{-2}$. Estimates of $\sigma_{\ell g} \sim 5 \times 10^{-16}$ cm^2 and $\sigma_{u\ell} \sim 5 \times 10^{-14}$ were obtained from the asymptotes and the value at 0.9 Torr. The latter is in reasonable agreement with Terenin and Prileshojewa's** value of $\sigma'_{u\ell} + \sigma'_{ug} = 2.0 \times 10^{-14}$ cm^2 for TℓI quenching the Tℓ $7^2S_{1/2}$ level. The surprising fact is that the TℓBr cross-section for quenching the upper Tℓ level ($7^2S_{1/2}$) is 100 times larger than that for the lower ($6^2P_{3/2}$).

With 3.5 Torr of TℓBr in the photodissociative tube, pressures up to 135 Torr of xenon were added. The addition of xenon increased n_u/n_ℓ by no more than a factor of 3. The addition of N_2 or CO_2 did not increase n_u/n_ℓ to 1. These discouraging results seem to indicate that it may be impossible to find a gas which selectively quenches the Tℓ $6^2P_{3/2}$ level.

The method of Ladenburg and Reiche as described in Mitchel and Zemansky*** and used in the experimental work just discussed, presupposes that the transition consists of a single component with a Doppler line shape. As indicated in Figure 8 the structure of the Tℓ 5350Å line is complex. Moreover above a few Torr, pressure broadening effects should be taken into consideration. It is possible to account for these effects by modifying the absorption coefficient in the integral expression for the "line absorption." However, to improve the accuracy of the measurement, a different approach is suggested; namely, to measure n_u-n_ℓ directly by utilizing a scanning

*Ibid, p. 118

**Ibid, p. 213

***Ibid, p. 118

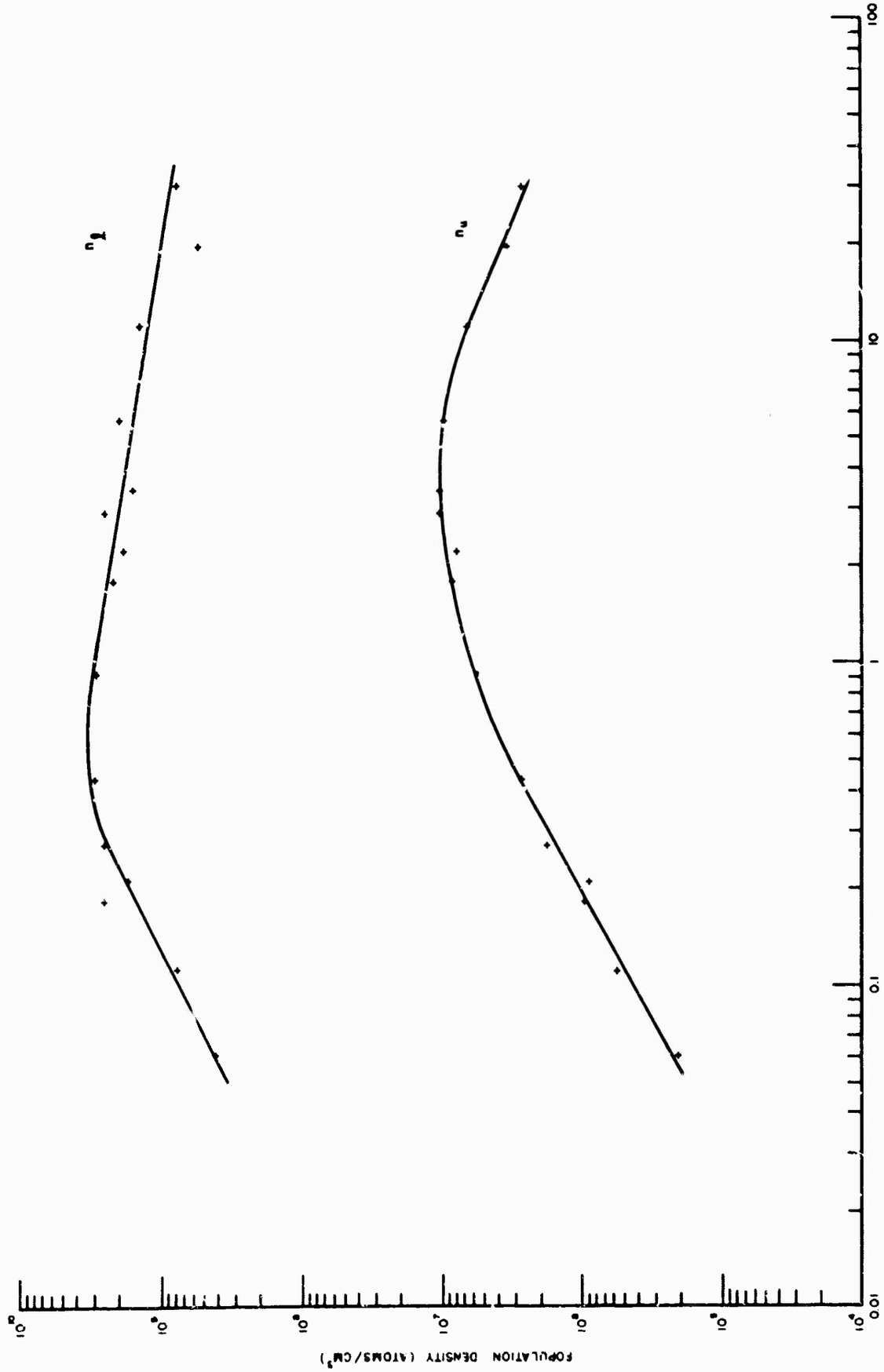

FIGURE 6. UPPER ($7^2S_{1/2}$) AND LOWER ($6^2P_{3/2}$) THALLIUM LEVEL POPULATION DENSITIES AS A FUNCTION OF THALLIUM BROMIDE VAPOR PRESSURE

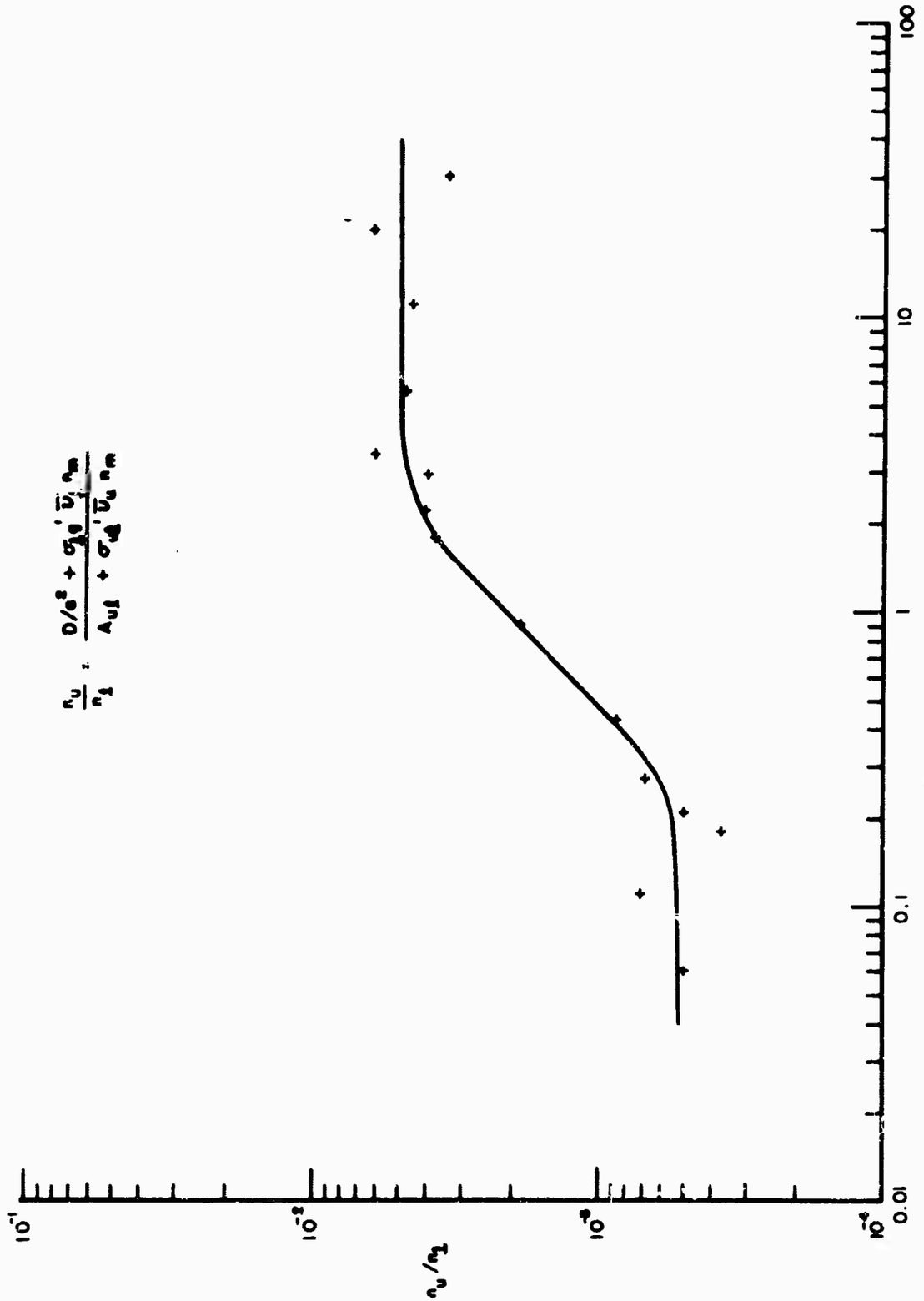

FIGURE 7. RATIO OF THE UPPER TO THE LOWER THALLIUM LEVEL POPULATION DENSITIES AS A FUNCTION OF THALLIUM BROMIDE VAPOR PRESSURE.

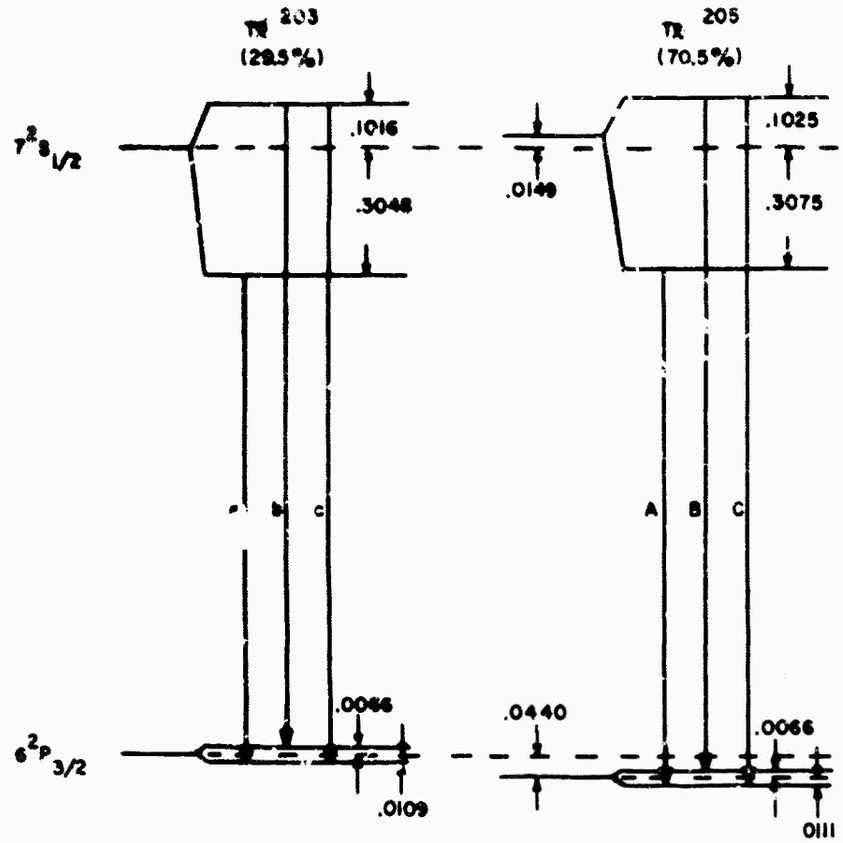

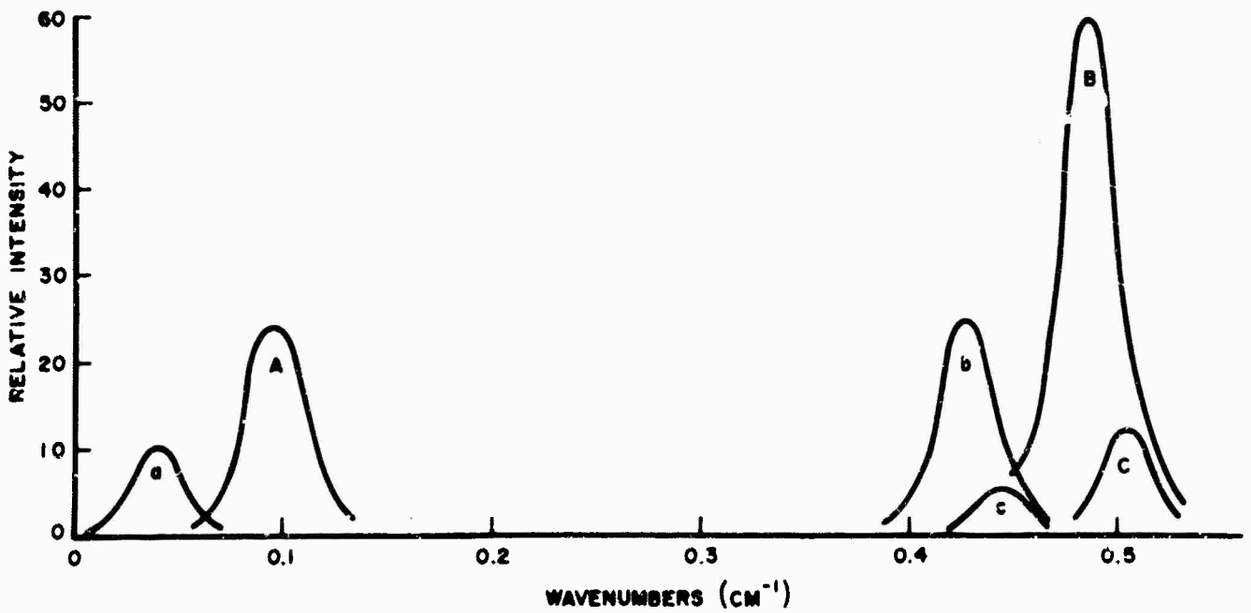

FIGURE 8. STRUCTURE OF THE THALLIUM 5350Å LINE.

Fabry-Perot interferometer* and separated Tl^{205} isotope to examine the line shape of component A (Figure 8) and compute $\int \kappa_\nu d\nu$. This measurement will probably not lead to the discovery of a quenching gas for Tl, but it would yield more accurate values of the various quenching cross-sections. Knowledge of these quenching cross-sections could provide a better understanding of several laser mechanisms including the collision laser.

Future Work

During the second half of this contract, the possibilities of a photodissociation laser in the cesium halides will be re-examined. A quenching gas is not required here.

*P. Jacquinot, in Reports on Progress in Physics, Vol. 23, A.C. Strickland, ed. (The Physical Society, London, 1960) p. 267.

5. THERMO-OPTICAL EFFECTS IN SOLID-STATE LASER MEDIA

Solid-state lasers, particularly ruby and glass: Nd, are capable of high peak power and high energy operation. However, the output radiance of these devices falls far short of the theoretical limits. An alternative way of expressing this result is that the output beam angles are approximately two orders of magnitude greater than the diffraction limit. Primary effort during this reporting period has been devoted to a fundamental study of those physical parameters which are instrumental in determining the spatial coherence of solid-state lasers.

The output radiance of solid-state lasers is strongly influenced by the optical quality of the host materials. Thus much effort in the past has been devoted to obtaining high optical quality laser rods. Particular success has been obtained with glass where the static optical quality is nearly perfect. However, as a result of flashlamp pumping, thermal gradients are introduced into the rods, and these in turn give rise to thermo-optical effects.

Using a Mach-Zehnder interferometer, time resolved interferograms were obtained during the pumping pulse. These interferograms were interpreted in terms of distortions of the optical path of the lasers under investigation. For both ruby and glass rods, distortions on the order of six wavelengths for a 15 cm rod were observed in the phase front of a plane wave propagating through the rods. One of the most significant aspects of this result is that the patterns were found to be repeatable from shot-to-shot, thus implying the possible use of optical correction. A detailed description of the experimental procedure and results is contained in a paper submitted for publication. A copy of this paper is included as Appendix A.

6. LASER PUMPING LASER

The purpose of this experiment is to investigate the utility of using a laser as a pumping source for a second laser. The basic idea is to reduce the heating of the laser medium usually associated with flashlamp pumping. Thus, the pumping laser represents a narrow band source, which since it is sufficiently close to the laser transition being pumped, will introduce negligible heating. The optical properties of the laser medium pumped in this fashion should therefore remain essentially constant.

The particular system chosen for this investigation utilizes two ruby lasers, the pumping laser oscillating in the R_2 line and the pumped laser oscillating in the R_1 line. The physical arrangement is illustrated in Figure 9.

The first stage laser produces an R_2-beam which is absorbed in the second stage ruby. As a result of this absorption the $^2E(2\bar{A})$ level is populated (Figure 10). The $^2E(2\bar{A})$ level couples rapidly by means of lattice vibrations to the $^2E(\bar{E})$ level. Since the lattice vibrations correspond to the crystal temperature, the populations of the levels $^2E(2\bar{A})$ and $^2E(\bar{E})$ assume a Boltzmann distribution at this temperature. For high pump intensity, the levels $^4A_2$ and $^2E(\bar{A})$ will approach equal populations. For sufficiently low ruby temperatures, the near equalization between the ground and the $^2E(2\bar{A})$ level, together with the Boltzmann distribution between the $2E(2\bar{A})$ and $^2E(\bar{E})$ levels, results in a population inversion between $^2E(\bar{E})$ and the ground level. Thus laser action can occur in the R_1 line. Since the ruby levels shift with temperature, both the first and second stage laser have to be kept at the same temperature.

The population inversion for the R_1 line in the second stage laser increases with the pump intensity and with the inverse of the temperature.

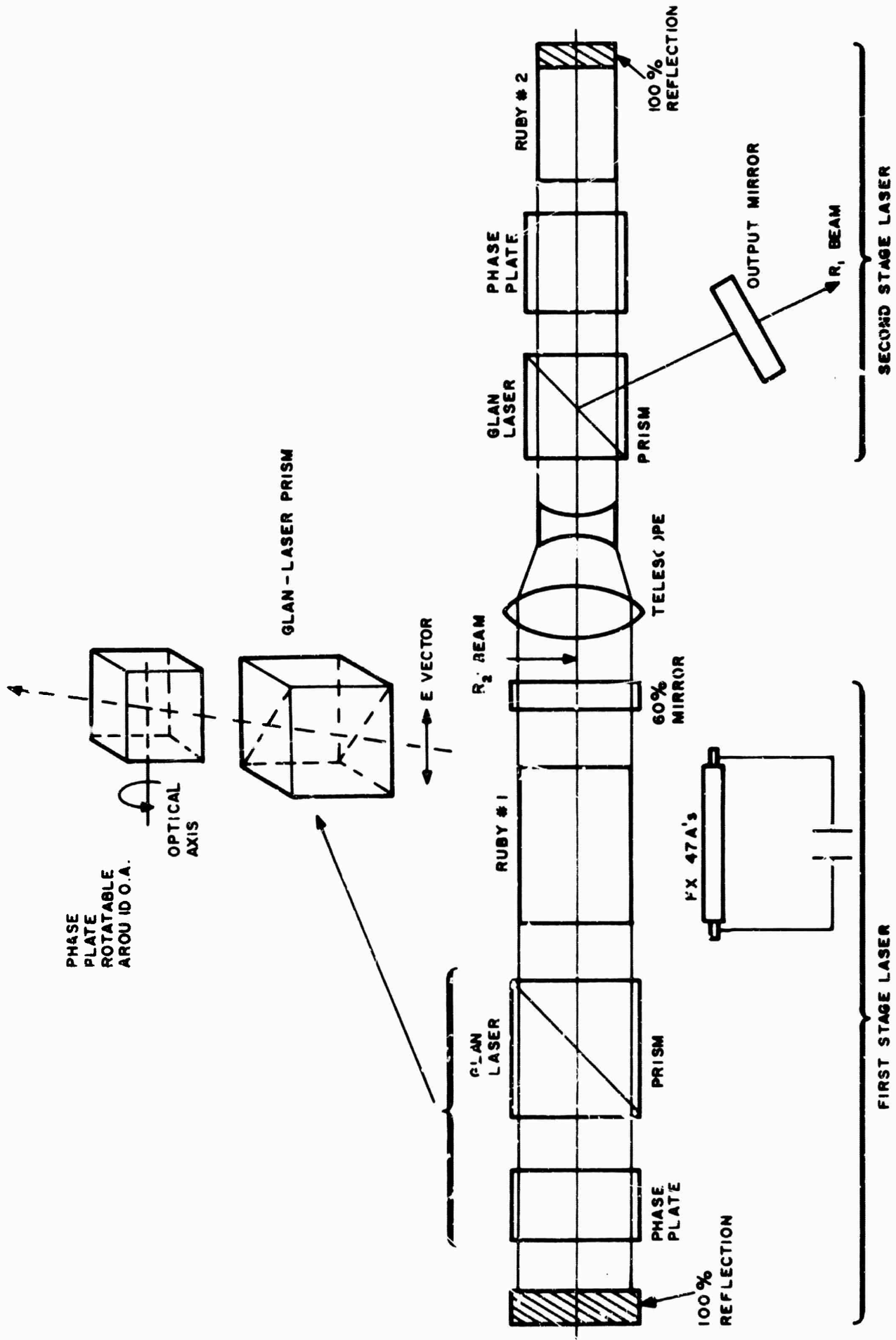

Figure 9. Optical Schematic of Two-Stage Laser

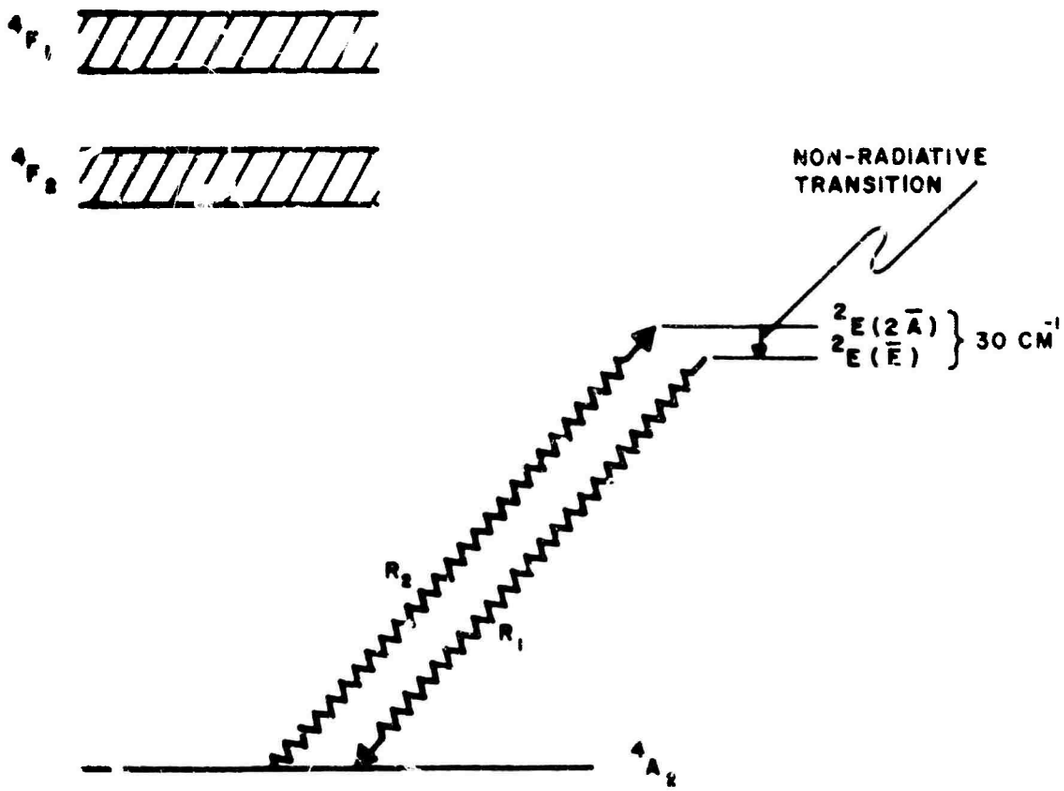

Figure 10. Ruby Energy Level Diagram

Experimental Design

The first stage laser uses a 1.5 cm diameter by 6 inch long cylindrical ruby which is pumped by two EGG-FX47 flashlamps in a pumping enclosure of double cylindrical geometry. Multilayer reflectors of 100% and 60% reflectivity represent the optical resonator. The R_2 operation of the first stage laser is achieved with the help of a Lyot-Oehman filter consisting of a polarizer, phase plate and the 100% mirror. The phase plate is a single quartz crystal whose thickness, d = 9.5 mm, was chosen such that it represents a $\lambda/4$ wave plate for the R_1-line and a $\lambda/2$ wave plate for the R_2 line.

The optical axis of the quartz forms a 45° angle with the electrical field of the light passing through the polarizer. The Lyot-Oehman filter has a spectral transmission characteristic of alternating stop and pass bands. The transmission T is equal to

$$T = \cos^2 (\pi(\Delta n/\lambda) d).$$

The thickness d is chosen such that

$$T = T_1 \text{ for } \pi(\Delta nd/\lambda_1) = (2N+1)\frac{\pi}{2} \qquad (A)$$

$$T = T_2 \text{ for } \pi(\Delta nd/\lambda_2) = N\pi \qquad (B)$$

where $\Delta n = n_e - n_\omega$

$\lambda_1 = R_1$ wavelength

$\lambda_2 = R_2$ wavelength

T_1 and T_2 are the transmissions for the R_1 and R_2 lines.

Obtaining the value of d from these equations, one finds d = 9.5 cm. This result is insensitive to ruby crystal temperature changes.

To tune in exactly for condition A, the phase plate was rotated lightly around its optical axis thus changing the effective thickness of the phase plate. The faces of the first stage

ruby were anti-reflection coated to prevent any oscillation between one of the faces and the output mirror which would naturally take place in the R_1 line.

It is desirable to cool the second stage crystal to as low a temperature as possible. However, since the first stage crystal must be at the same temperature, there are some limitations to be observed.

(1) Since the gain of the ruby laser increases with the decreasing temperature, it is necessary to set a lower limit to the temperature of the crystal in order to prevent an excessive amplification of spontaneous emission which would tend to depopulate the upper laser level.

(2) Another limitation is defined by the performance of the filter. For R_2-laser operation, two conditions have to be fulfilled:

$$T_1 < \frac{1}{R} e^{-2\ell\alpha_1} = \tau_1$$

$$T_2 > \frac{1}{R} e^{-2\ell\alpha_2} = \tau_2$$

T_1 = filter transmission at the R_1 frequency

T_2 = filter transmission at the R_2 frequency

α_1 = gain coefficient for R_1 radiation

α_2 = gain coefficient for R_2 radiation

R = reflectivity of the output mirror

ℓ = crystal length.

Table 1 shows τ_2/τ_1 as a function of temperature. From that table we can see that the filter contrast T_2/T_1 has to increase with decreasing temperature.

Temperature	τ_2/τ_1
300°K	2
200°K	6
160°K	50
100°K	2000

Table 1. τ_2/τ_1 vs Temperature for $\frac{1}{2}$ inch long ruby

The first stage laser delivers an R_2 laser beam which is sent through a demagnifying telescope in order to increase its energy density. As is discussed in more detail in Appendix B, an energy density of at least 4 joules/cm^2 is required for sufficient pumping of the second stage laser rod at dry ice temperatures.

The set up is shown in Figure 9. The vertically polarized R_2 light passes through a Glan polarizer and enters a quartz phase plate which constitutes a full wave plate for the R_2 line and a half wave plate for the R_1 beam. Therefore, the R_2 beam leaves the phase plate with the same vertical polarization with which it entered the plate.

The second stage laser oscillates in the R_1 line. The second stage ruby is a 60 degree rod, i.e., the c-axis forms an angle of 60° with the cylinder axis. It is, therefore, necessary that the R_1 as well as the R_2 light beams are polarized normal to the plane defined by the c-axis and cylinder axis.

A vertically polarized R_1 beam emerges from the second stage ruby rod, enters the phase plate and leaves it horizontally polarized. In the Glan Prism, the horizontally polarized R_1 beam is reflected off the interface, leaves the prism at an angle of 117° to the system axis and intercepts the output mirror. It is returned back through the prism and phase plate and re-enters the crystal with the correct polarization.

Future Work

The necessary optical, mechanical, and electrical components are under construction. The entire apparatus will be placed in a dry box to prevent frosting. Cooling will be provided by cold nitrogen gas flowing over the crystals. It is planned to operate and optimize the performance of the first stage R_2 laser before using it as a pump source for the R_1 laser.

APPENDIX A

DYNAMIC OPTICAL PATH DISTORTIONS IN LASER RODS

DYNAMIC OPTICAL PATH DISTORTIONS IN LASER RODS*

by

S. D. Sims
A. Stein
C. Roth

INTRODUCTION

All of the important output characteristics of a laser can be determined from a knowledge of the phase and amplitude distribution of the field across the exit aperture. This distribution is dependent upon many factors involving the components and geometry of the laser system. The optical quality of the components within the laser resonator is certainly an important factor. In solid state devices, the laser rod itself should be of the highest possible optical quality in order to obtain the most optimum output characteristics. Much recent effort has been devoted to the problem of obtaining such rods, either crystals or glass. Since high energy and/or high power devices are of interest, most of the work has been devoted to obtaining improved quality ruby crystals or improved glass laser material doped with Neodymium. It is these materials which were treated in the experiments reported here.

The term "optical quality" is somewhat vague, and so it is useful to point out here just what optical properties of the material are important for lasers. Generally speaking, the expression is used to denote two broad areas:

*The work described in this article was supported by project Defender, sponsored by Advanced Research Agency Department of Defense and technically monitored by the Air Force Office of Scientific Research under Contract AF49(638)-1535 and by the Office of Naval Research under Contract Nonr-3833(00).

a) Those material parameters which contribute to an attenuation of a light beam, such as the density of scattering or absorbing centers; and

b) Variations of the refractive index which lead to wavefront distortions of a transmitted beam.

Although excellent quality rods have been fabricated, these rods do not maintain their quality when subjected to the intense pump light used in high power lasers. The distortions are introduced as a result of the existence of thermal gradients which evolve during the pumping pulse. The thermal gradients and resultant optical distortion may actually increase after the end of the pumping pulse as a result of the cooling process. The magnitude and time scales of the thermal gradients are of course related to material parameters. Since laser action only occurs during the pumping pulse (or shortly thereafter in the case of Q-switching) the main interest is centered around the time interval of the pumping pulse. However, due to the cumulative nature of the gradients, there may be some interest in times long compared to the pumping pulse for high repetition rate systems.

EXPERIMENTAL DESCRIPTION

Fringe Patterns

Standard procedures for measurement of optical distortion make use of interferometric techniques. A Mach-Zehnder interferometer (M-Z) was chosen for this application since it allows measurement of single pass properties. Thus the laser rod under investigation is inserted in one arm of the M-Z while the other arm is

an air path. Then a plane wave entering the rod undergoes distortions in the rod such that the surface of constant phase is no longer a plane, but a curved surface. The curvature of this surface is indicated by changes in the fringe pattern which occur when the sample beam is recombined with the reference beam. Since this pattern will be changing in time, it is necessary to sample the pattern in order to obtain time resolved information.

In these experiments, a Q-switched laser was used as the interferometer illumination source. Since the output of this laser is a 30 nanosecond pulse, the resultant interferograms were resolved to 30 nanoseconds. The electronic circuitry was such that the time of occurrence of the probe pulse could be adjusted to occur at any desired time with respect to the initiation of pumping of the test rod. Time resolved interferograms were obtained for two cases:

A) The sample was a Nd - glass rod. For this case a Q-switched ruby laser was used as the probe.

B) The sample was a ruby rod. For this case a Q-switched Nd - glass laser was used as the probe.

The wavelength of the probe light differs significantly from the laser wavelength of the sample in either case, and hence the regions of anomolous dispersion are avoided.

The experimental setup is schematically illustrated in Figure 1.

Case A:

The light source is a Q-switched ruby laser. It provides a single, linearly polarized, 0.3 joule pulse of 30

nsec duration, subsequently referred to as the "probe light." The probe light is reflected off a Schott UG-8 glass plate close to Brewster's angle in order to achieve appropriate attenuation. It then passes through a telescope of magnification M=4 and enters the M-Z, where it is split into two parts of equal intensity at the semi-reflecting surface A_1. The two beams are then reflected off the mirrors M_1, M_2, and recombined at the semi-reflecting surface A_2. The beam splitters, D_1, D_2 are adjusted such that the second surfaces B_1 and B_2 are at Brewster's angle for the probe light, thus eliminating second surface reflection. If all reflecting surfaces are exactly parallel, a plane wave going through the M-Z would give fringes at infinity.

In general however, the wave fronts of the two beams are mutually inclined and the light forms fringes parallel to their intersection. By adjusting M_1, M_2, D_1 or D_2 one can change the fringe-density. It is these fringes that are used in the examination of the laser rod samples.

A Corning Code 0850 Nd-glass rod of 15 cm length and 1.5 cm diameter was placed in one arm of the M-Z. This crystal was mounted in a laser head, consisting of two EGG-FX47A flashlamps and a focusing reflector of double cylindrical geometry. The flashlamps were driven by a PFN which delivered 7000 joules into the lamps during a 2.3 msec long pulse.

As was described above, the optical pathlength of the sample will undergo changes during and after the flashlamp pulse due to heating of the sample. This results in a change of the interferogram obtained with the M-Z .

The beam divergence of the light source was 3×10^{-3} rad corresponding to an area of coherence in the beam cross section of .2 mm diameter. The telescope increased the coherence area in the beam cross section to 0.8 mm in diameter. Therefore, one could allow shear on the order of 1/10 mm between the two beams in the M-Z without extinguishing the fringe visibility.

The telescope had the additional advantage of beam expansion, thus allowing complete filling of the glass rod aperture.

Case B:

The light source is a Q-switched Nd-glass laser which provides an 0.3 joule pulse of 30 nsec duration, the probe light. This time the probe light was reflected off a dielectric coated Quartz flat near Brewster's angle such that almost linear polarization of the probe light was obtained. The M-Z was used in the same setup as for Case A. The limited temporal coherence of the Q-switched Neodymium glass laser can be described in terms of a coherence time $\tau = 3 \times 10^{-12}$ sec corresponding to a linewidth of 100 Å and a coherence length in the longitudinal direction of 0.1 mm. The optical axis of the ruby was at 60° to the cylinder axis and the polarization of the probe was normal to the optical axis, so that the polarization was the same as that of an oscillating crystal. The ruby crystal rod of 15 cm length and 1.5 diameter introduced an additional optical path length of over 11 cm which had to be balanced by inserting an adjustable compensator* in the other arm. The interferomgrams obtained at different time instances during the pumping pulse were photographed with Kodak IR- film plates.

*To be published in Journal of Appl. Opt.

The series of interferograms obtained in Cases A and B are shown in Figures 2A and 2B.

Fringe Counting

The interferograms described above show only the relative change in optical path length across the aperture. In order to determine the absolute change in optical path length, a fringe counting experiment was performed. The experimental arrangement is illustrated in Figure 3. The light source is a He-Ne gas laser. The telescope expands the beam so that it fills the sample aperture. After passing the M-Z with the inserted sample the light beam forms a fringe structure which is intercepted by a beam-splitter BS. The two fringe pattern F_1 and F_2 are intercepted by screens with 1 mm pinholes. One pinhole is located in the center of the fringe pattern, the other at the edge of the pattern. Behind the pinholes are RCA 6342Å photomultipliers with narrow-band transmission interference filters centered at 6328Å. The photomultiplier outputs are displayed on a Tektronix 555 oscilloscope and photographed with a scope camera (Figure 4).

DISCUSSION OF RESULTS

The series of interferogram in Figures 2A and 2B show the development of a whirlpool fringe structure with the center on the right hand side. These fringes are the geometrical loci of constant optical path lengths. The fringe patterns are somewhat confusing since a bias is introduced by the initial tilt of the M-Z interferometer. A mapping can be performed to translate

the fringe structure into the shape of a surface of constant phase by removing the bias. This surface then represents the distortion of a plane wave. A cut is taken through the region of maximum distortion and the resulting path length in the plane of the cut is plotted in Figure 5. Curve A is a plot of the raw data, B is the bias, and C represents the shape of the wavefront. The curves of Figure 5 are for the glass rod at time T = 2.4 ms. A similar plot for the case of ruby is presented in Figure 6. As can be seen fron Figures 5 and 6, the distortion of the optical path is lens-like and represents the single pass variation across the aperture of an initially plane wave.

The interferograms determine only the relative changes in path length. Moreover, they provide no information as to whether the surface of constant phase is concave or convex. In order to determine this additional information, the fringe counting experiment described above was performed. It is reasonable to assume that heating of a rod will lead to a net increase in optical path length. The oscilloscope traces of Figure 4 show that during the pumping pulse, the edge of the aperture undergoes a greater expansion than the center. Thus the optical path is actually concave, and the rod will behave like a negative lens. The implication is that the heat deposition is such that it leads to higher temperatures at the outer edge of the rods. The shape of the curves of Figures 5 and 6 took this result into account.

The bulk temperature rise of the laser rods can be calculated from the results of the fringe counting experiments. For a laser rod of length, s, and index of refraction, n, inserted in

an arm of the interferometer of length, L, the net optical path length, P, of the interferometer arm can be written as

$$P = ns + (L-1) = (n-1)\, s + L.$$

The corresponding change of path length with temperature is then,

$$\frac{\Delta P}{\Delta T} = (n-1)\,\frac{ds}{dT} + s\frac{dn}{dT}$$

where $\frac{ds}{dT} = \alpha s$; α = linear expansion coefficient and $\frac{dn}{dT}$ = index variation with temperature. Thus

$$\Delta T = \frac{\Delta P}{s\left[(n-1)\,\alpha + \frac{dn}{dT}\right]}$$

For the glass laser rod

$$s = 15 \text{ cm}$$

$$n = 1.533$$

$$\frac{dn}{dT} = .2 \times 10^{-5}/°C$$

$$\alpha = 10^{-5}/°C$$

and from Figure 4A

$$\Delta P = 10\lambda = 7 \times 10^{-4} \text{ cm}$$

$$\therefore \Delta T(\text{glass}) = 6.4°C$$

For the ruby rod,

$$s = 15 \text{ cm}$$

$$n = 1.76$$

$$\frac{dn}{dT} = 1.1 \times 10^{-5}/°C$$

$$\alpha = .5 \times 10^{-5}/°C$$

$$\Delta T = 32\lambda = 33.9 \times 10^{-4} \text{ cm}$$

and

$$\Delta T(\text{ruby}) = 15.3°C.$$

These results are in agreement with independent thermocouple measurements of the bulk temperature rise. The magnitude of the thermal gradients cannot be inferred from the wavefront distortion since, due to the existance of internal stresses, the expansion is not uniform along the rod length.

CONCLUSIONS

From the results of the above experiments, it is clear that significant thermal distortions are introduced during the pumping cycle. A Q-switched laser is a highly effective interferometer illumination source in cases where high time resolution is desired. One of the side benefits accruing from the use of such a technique is the observation that the results are highly reproducible from shot to shot. Thus optical correction can be employed to improve resonator performance at any desired time. This is particularly useful in the case of Q-switching where the resonator characteristics need only be good during the development of the output pulse. Even for a normal pulse occurring over a time interval of milliseconds, correction may be used to improve the time averaged resonator characteristics. The correct optical figure for a compensating plate can be computed directly from the interferograms.

The authors would like to thank Mr. T. Shultz and Dr. R. T. Daly for many interesting and helpful discussions.

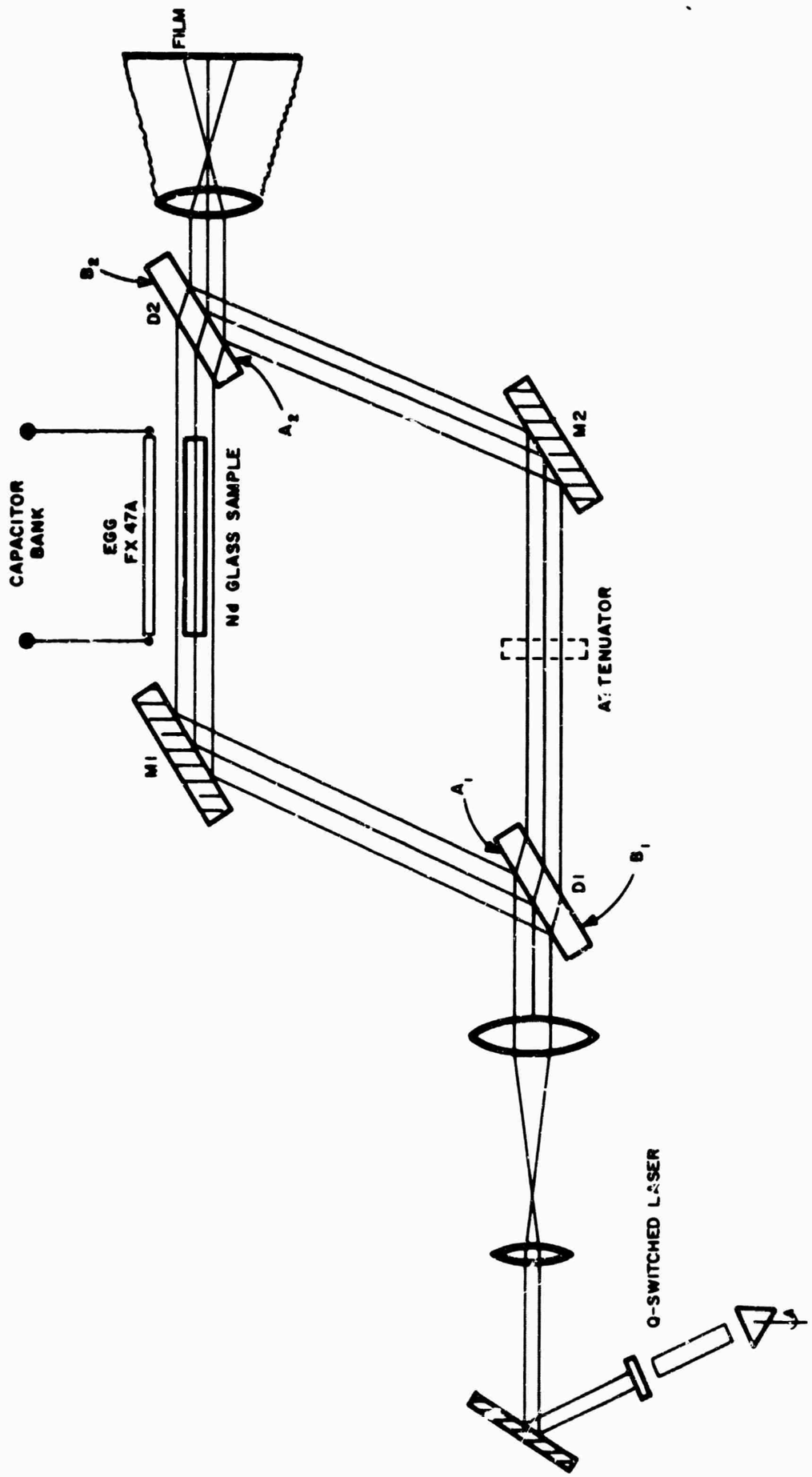

FIGURE 1. MACH-ZEHNDER-INTERFEROMETER

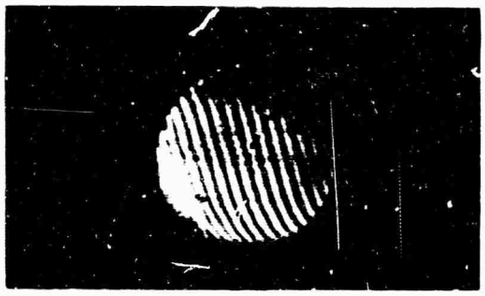

a. Air (No rod in M-Z)

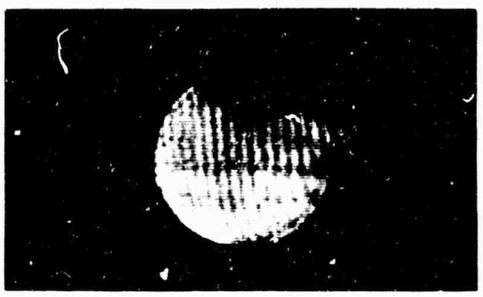

b. t = 0 (Rod in)

c. t = 200 μsec

d. t = 700 μsec

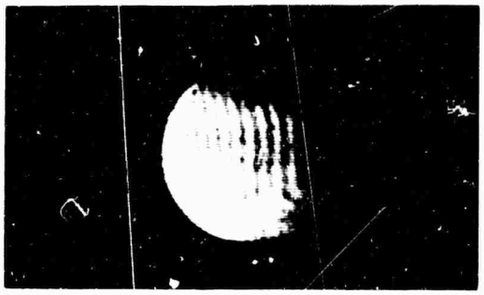

e. t = 1200 μsec

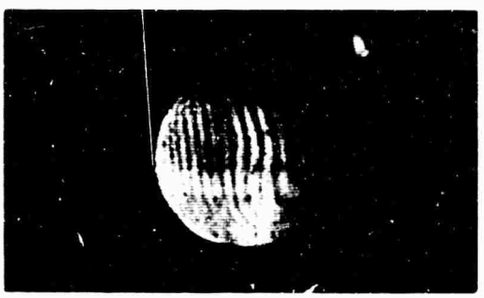

f. t = 1700 μsec

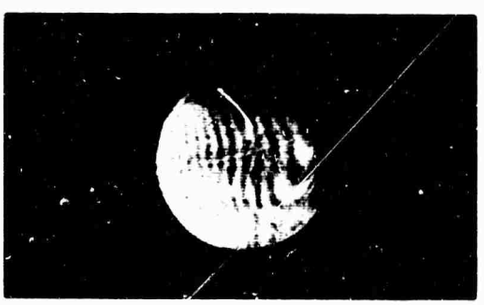

g. t = 2200 μsec

h. t = 2,700 μsec

FIGURE 2A GLASS LASER ROD INTERFEROGRAMS AT DIFFERENT TIMES

Note: t = 0 corresponds to start of pump pulse

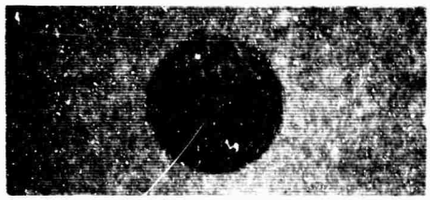

(A) t = 0

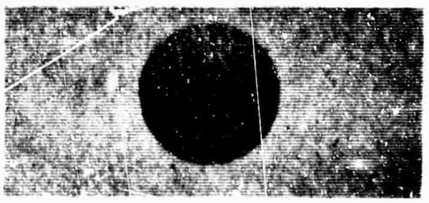

(D) t = 1.4ms

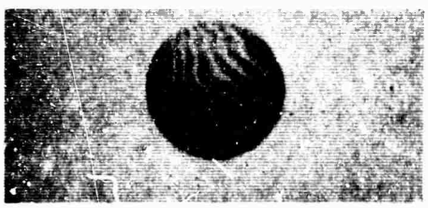

(B) t = .4mc

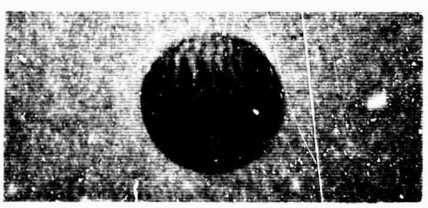

(E) t = 1.9ms

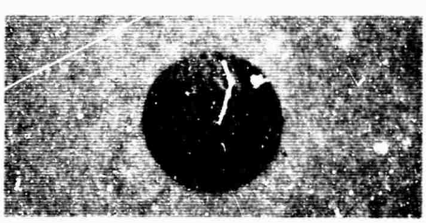

(C) t = .9ms

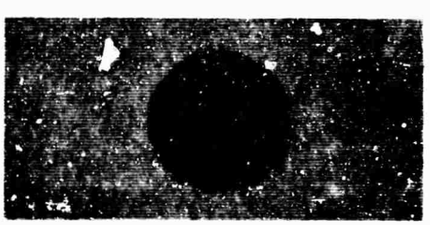

(F) t = 2.4ms

NOTE: t = 0 CORRESPONDS TO START OF PUMP PULSE

Figure 2b. Ruby Laser Rod Interferograms at Different Times

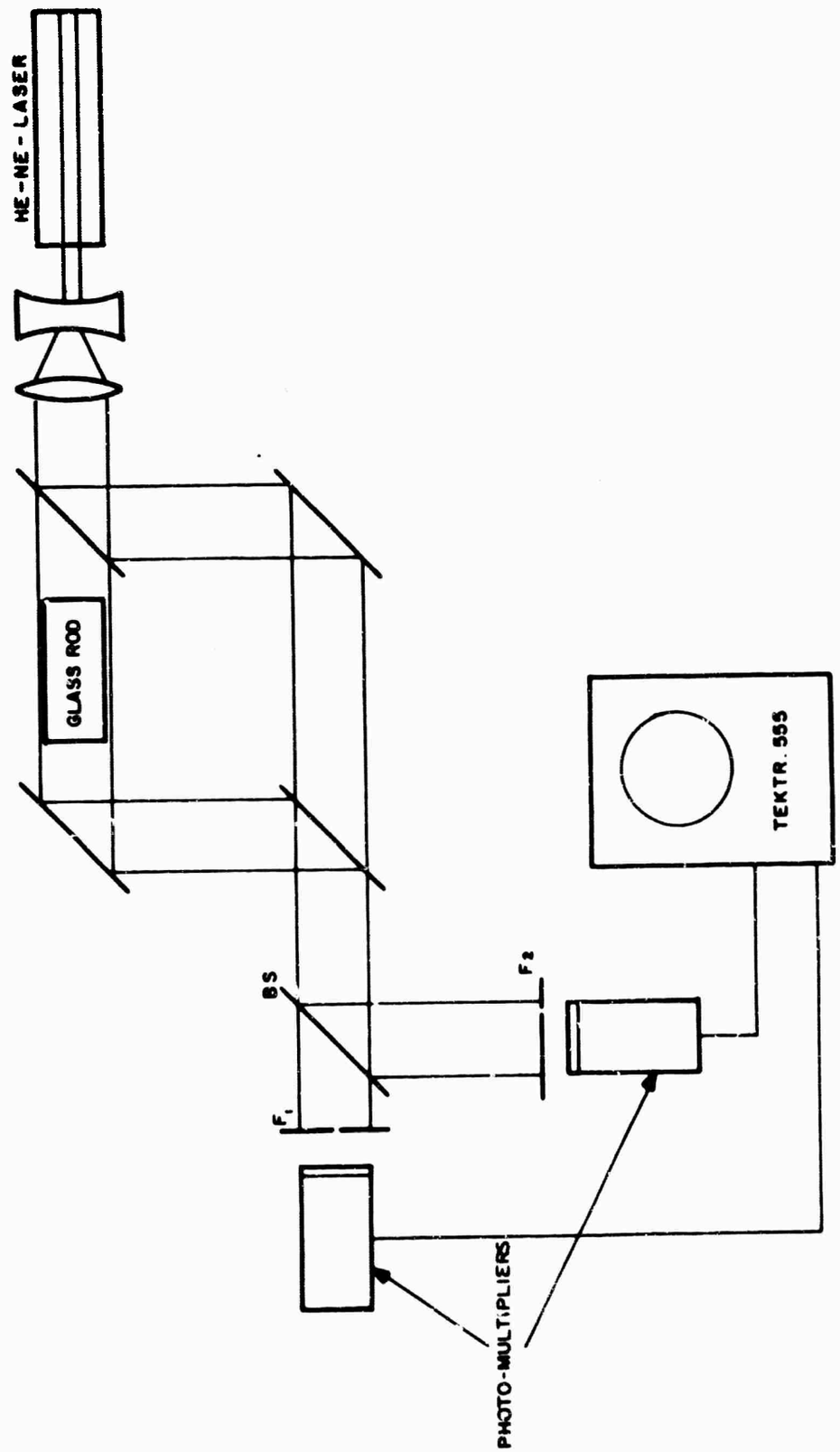

FIGURE 3. FRINGE COUNTING EXPERIMENT

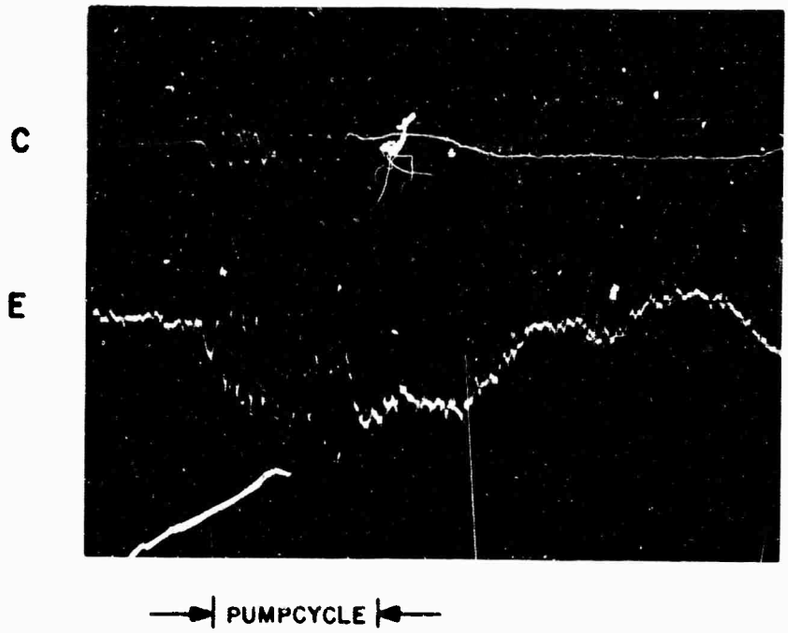

Figure 4a. Change in Path Lengths at Center and Edge of Glass Rod During Pumping

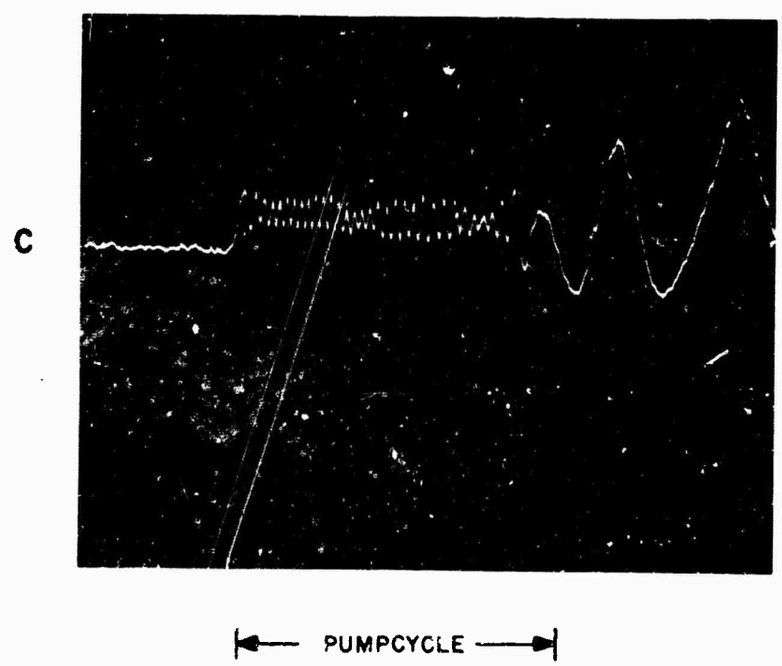

Figure 4b. Change in Path Length at Center of Ruby Rod

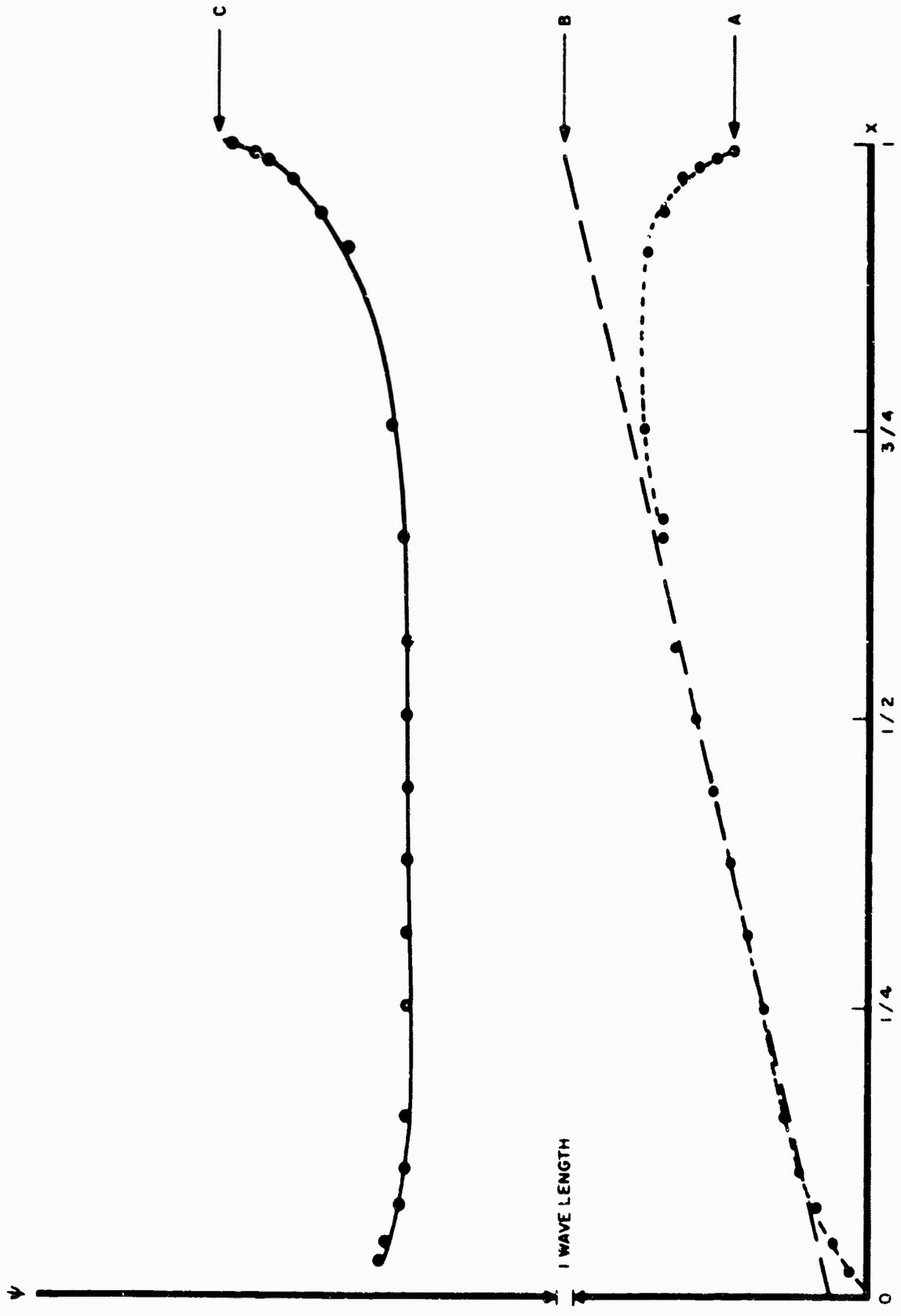

FIGURE 5. MAPPING OF FRINGE PATTERN ACROSS APERTURE OF GLASS ROD

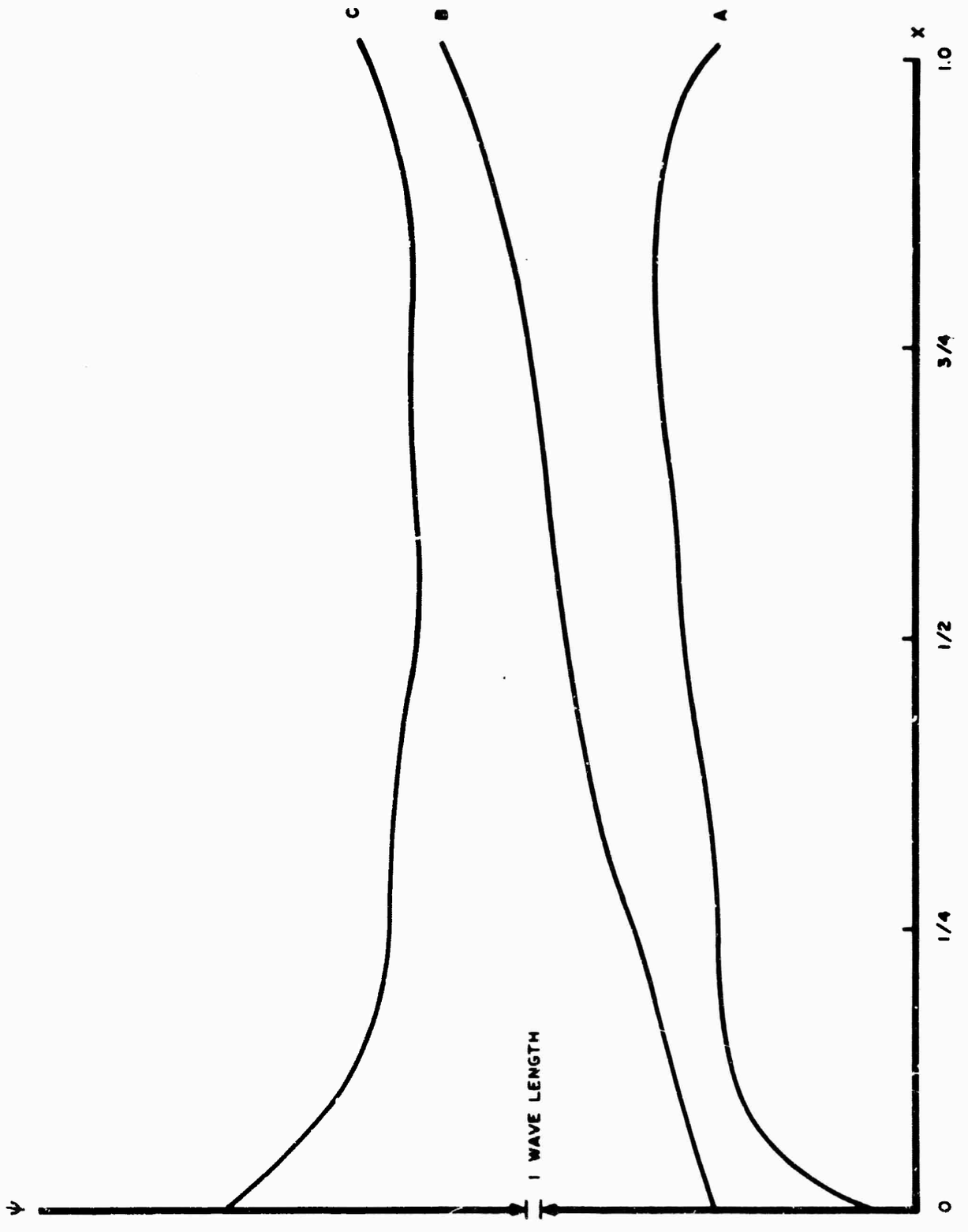

FIGURE 6. MAPPING OF FRINGE PATTERN ACROSS APERTURE OF RUBY ROD

APPENDIX B

END PUMPING OF AN R_1 RUBY LASER BY AN R_2 RUBY LASER

This appendix considers the problem of pumping a ruby laser through the R_2 line by irradiating the end of a ruby rod with the output of another ruby laser oscillating in the R_2 line. A schematic of the arrangement is shown in Fig. 1.

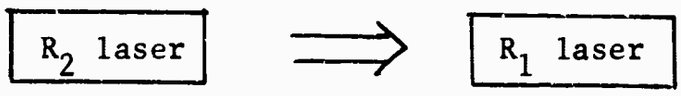

Figure 1.

1.0 General Analysis

In order to simplify the analysis, the problem is approached for the case of no oscillation in the R_1 laser. Thus no clamping of the gain of this laser is provided due to the existence of an oscillation threshold. The population in the R_1 laser will be functions of position and time. The situation is depicted in Fig. 2.

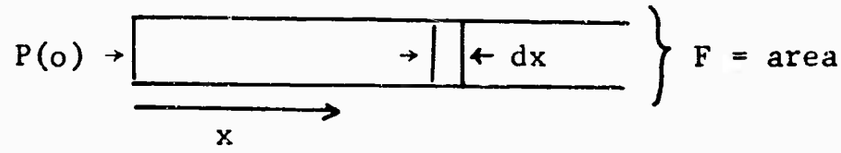

Figure 2.

Here, the pumping rate at the end of the rod is P(o) and is assumed constant in time and uniform over the cross-section of the rod. At a distance x down the rod, the pumping rate is P(x,t), i.e., it is a function of position and time.

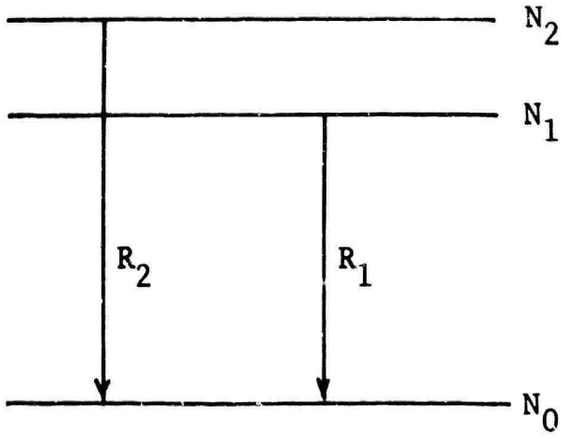

Figure 3.

A simplified energy level diagram is shown in Fig. 3, where the N's represent the populations of the states and the ground state splitting is ignored. The pumping equation for an R_2 pump can then be written as

$$\frac{dN_0(x,t)}{dt} = P(x,t)g_o\left[\frac{N_2(x,t)}{g_2} - \frac{N_0(x,t)}{g_o}\right] + AN_1(x,t) + AN_2(x,2) \qquad (1)$$

where g_i = degeneracy of the i^{th} state $(i = 0,1,2)$

A = Einstein coefficient

The pumping rate $P(x,t)$ can be related to the power flux $I(x,t)$ by

$$P(x,t) = \frac{I(x,t)\sigma_{02}}{h\nu_2} \qquad (2)$$

where $I(x,t)$ = power flux (watts/cm^2)

σ_{02} = absorption cross-section for the R_2 line

$h\nu_2$ = energy of an R_2 line photon

An equation governing the x dependence of I(x,t) and can now be written as

$$\frac{dI(x,t)}{dx} = \sigma_{02}\, g_o \left(\frac{N_0(x,t)}{g_o} - \frac{N_2(x,t)}{g_2} \right) I(x,t) \ , \qquad (3)$$

or in terms of P(x,t)

$$\frac{dP(x,t)}{dx} = \sigma_{02}\, g_o \left(\frac{N_2(x,t)}{g_2} - \frac{N_0(x,t)}{g_o} \right) P(x,t) \ . \qquad (4)$$

The absorption coefficient $\alpha_{02}(x,t)$ is now defined as

$$\alpha_{02}(x,t) = \sigma_{02}\, g_o \left(\frac{N_0(x,t)}{g_2} - \frac{N_0(x,t)}{g_o} \right) \ . \qquad (5)$$

Using this definition, Eq. (4) can be rewritten as

$$\frac{dP(x,t)}{dx} = \alpha_{02}(x,t)\ P(x,t) \ . \qquad (6)$$

It is of course clear that for the situation under discussion,

$$\alpha_{02} < 0 \ .$$

It is assumed that thermalization between levels 1 and 2 occurs sufficiently rapidly so that they may always be considered to be in thermal equilibrium, thus

$$\frac{N_2}{N_1} = e^{-\Delta E/kT} = a \qquad (7)$$

where ΔE = energy difference between levels 1 and 2
k = Boltzmann's constant
T = temperature (°K)

Defining the total number of atoms per cubic centimeter, S, we have

$$S = N_0(t,x) + N_1(t,x) + N_2(t,x) + N_0(t,x) + ((1+a)/a)N_2(t,x) \quad (8)$$

Eq. (5) and (8) can be used to obtain expressions for $N_2(x,t)$ and $N_0(x,t)$. Thus,

$$N_2(x,t) = \frac{\alpha_{02}(x,t) + \sigma_{02}S}{\sigma_{02}\left[\frac{g_o}{g_2} + \frac{(1+a)}{a}\right]} \quad (9)$$

and

$$N_0(x,t) = S - \frac{\alpha_{02}(x,t) + \sigma_{02}S}{\sigma_{02}\left[\frac{g_o a}{g_2(1+a)} + 1\right]} \quad (10)$$

Defining

$$K = \frac{g_o}{g_2}\frac{a}{(1+a)} + 1$$

and substituting Eq. (9) and (10) into Eq. (1) one gets

$$-\frac{d\alpha_{02}(x,t)}{dt} = KP(x,t)\,\alpha_{02}(x,t) + A\,\alpha_{02}(x,t) + A\,\sigma_{02}S. \quad (11)$$

Eq. (6) can be integrated to yield

$$P(x,t) = P(o,t)\left[\exp\left(\int_o^x \alpha_{02}(x,t)dx\right)\right] .$$

We will assume the R_2 pumping input is constant in time, so that

$$P(o,t) = P(o,o) = P_o ,$$

and thus

$$P(x,t) = P_o\left[\exp\left(\int_o^x \alpha_{02}(x,t)dx\right)\right] \quad (12)$$

This result can now be inserted into Eq. (11) to obtain

$$-\frac{d\alpha_{02}(x,t)}{dt} = KP_o\left[\exp\left(\int_o^x \alpha_{02}(x,t)dx\right)\right]\alpha_{02}(x,t) + A\alpha_{02}(x,t) + A\sigma_{02}S \quad . \tag{13}$$

2.0 Steady State Solution

This final equation obtained in the previous section is difficult to solve in the general case. However, the steady state case, $t \to \infty$ can be solved by setting

$$\frac{d\alpha_{02}}{dt} = 0 \quad ,$$

from which it follows that

$$\int_o^x \alpha_{02}(x)dx = \ell n\left\{\frac{(\alpha'_{02}/\alpha_{02}) - 1}{K(P_o/A)}\right\} \quad , \tag{14}$$

where $\alpha'_{02} = -\sigma_{02}S$ = unpumped absorption coefficient.

Eq. (14) can be converted into a differential equation in P(x) since, from Eq. (6)

$$\alpha_{02}(x) = \frac{1}{P(x)}\frac{dP(x)}{dx} \quad .$$

Inserting this into Eq. (14) and integrating, one obtains,

$$\frac{K}{A}(P_o - P(x)) + \ell n\left|\frac{P_o}{P(x)}\right| = \sigma_{02}\, S(x)$$

or

$$K\left(\frac{P_o}{A}\right)\left\{1 - \left[\exp\left(\int_o^x \alpha(x)dx\right)\right]\right\} - \int_o^x \alpha(x)dx = \alpha'_{02}(x) \ . \qquad (15)$$

By inserting Eq.(14) into Eq. (15) a transcendented expression for $\alpha(x)$ is obtained. Thus

$$x = -\frac{1}{\alpha'_{02}}\left[1 + K\left(\frac{P_o}{A}\right) + \ell n\ K\left(\frac{P_o}{A}\right)\right] + \left[\frac{1}{\alpha_{02}} + \frac{1}{\alpha'_{02}}\ \ell n\ \left(\frac{\alpha'_{02}}{\alpha_{02}} - 1\right)\right] \qquad (16)$$

$t = \infty$.

Several plots of $\alpha_{02}(x)$ vs x for different values of $\frac{P_o}{A}$ and for $T = 77°K$ are presented in Fig. 4.

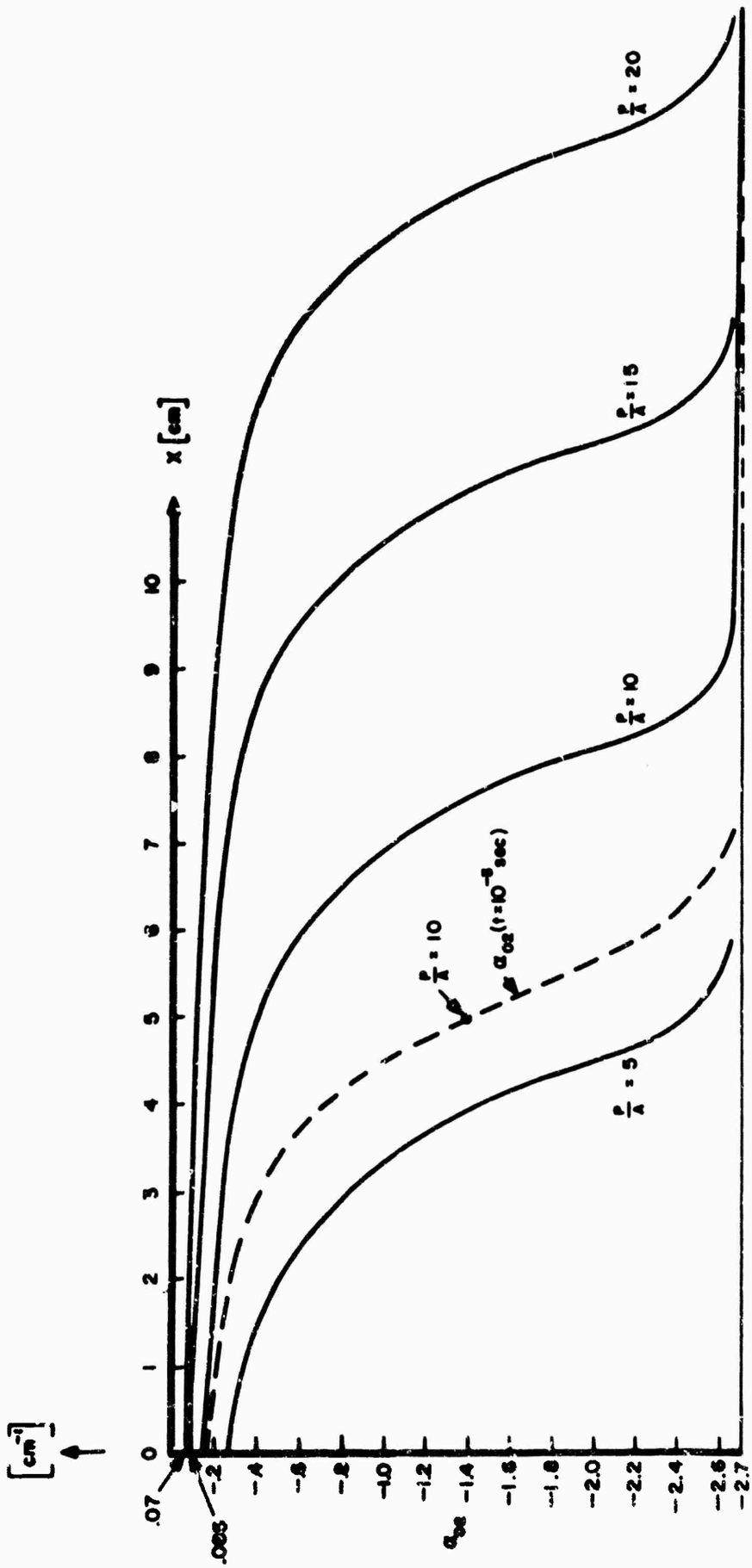

Figure 4. Absorption of R_2 Line in Ruby T_2 77°K

Unclassified
Security Classification

DOCUMENT CONTROL DATA · R&D

(Security classification of title, body of abstract and indexing annotation must be entered when the overall report is classified)

1. ORIGINATING ACTIVITY (Corporate author)	2a. REPORT SECURITY CLASSIFICATION
TRG Incorporation, A Subsidiary of Control Data Corporation, Route 110, Melville, N.Y.	Unclassified
	2b GROUP

3. REPORT TITLE

RESEARCH ON PROPERTIES OF LASER DEVICES

4. DESCRIPTIVE NOTES (Type of report and inclusive dates)

1st Technical Summary Report

5. AUTHOR(S) (Last name, first name, initial)

S. Jarrett, M. Piltch, C. Roth, B. Senitzky, S.D. Sims, A. Stein and W. Walter

6. REPORT DATE	7a. TOTAL NO. OF PAGES	7b. NO. OF REFS
15 Nov. 1964 through 15 May 1965	66	

8a. CONTRACT OR GRANT NO.	9a. ORIGINATOR'S REPORT NUMBER(S)
AF 49(638)-1535	
b. PROJECT NO. 5730	
c. Code No. 356	9b. OTHER REPORT NO(S) (Any other numbers that may be assigned this report)
d.	

10. AVAILABILITY/LIMITATION NOTICES

11. SUPPLEMENTARY NOTES	12. SPONSORING MILITARY ACTIVITY
	Advanced Research Projects Agency and Air Force Office of Scientific Research

13. ABSTRACT

Experimental work on gaseous and solid-state laser development is reported. The high temperature Mn collision laser tests indicated that insufficient gain was achieved to obtain oscillation with present apparatus. Experiments testing La and Y as collision laser media were concluded after demonstrating that higher discharge currents and higher operating temperatures than presently available were required. The possibility that photodissociation of TlBr in the presence of a quenching gas could lead to a population inversion was experimentally investigated. Mach-Zehnder interferograms of the transient optical path distortions introduced by optical pumping of ruby were obtained. An R_1 ruby laser pumped by an R_2 ruby laser experiment was designed and the construction of the apparatus initiated.

DD FORM 1 JAN 64 1473

Unclassified
Security Classification

14. KEY WORDS	LINK A		LINK B		LINK C	
	ROLE	WT	ROLE	WT	ROLE	WT
Lasers Gas Discharges Solid-State Physics						

INSTRUCTIONS

1. ORIGINATING ACTIVITY: Enter the name and address of the contractor, subcontractor, grantee, Department of Defense activity or other organization *(corporate author)* issuing the report.

2a. REPORT SECURITY CLASSIFICATION: Enter the overall security classification of the report. Indicate whether "Restricted Data" is included. Marking is to be in accordance with appropriate security regulations.

2b. GROUP: Automatic downgrading is specified in DoD Directive 5200.10 and Armed Forces Industrial Manual. Enter the group number. Also, when applicable, show that optional markings have been used for Group 3 and Group 4 as authorized.

3. REPORT TITLE: Enter the complete report title in all capital letters. Titles in all cases should be unclassified. If a meaningful title cannot be selected without classification, show title classification in all capitals in parenthesis immediately following the title.

4. DESCRIPTIVE NOTES: If appropriate, enter the type of report, e.g., interim, progress, summary, annual, or final. Give the inclusive dates when a specific reporting period is covered.

5. AUTHOR(S): Enter the name(s) of author(s) as shown on or in the report. Enter last name, first name, middle initial. If military, show rank and branch of service. The name of the principal author is an absolute minimum requirement.

6. REPORT DATE: Enter the date of the report as day, month, year, or month, year. If more than one date appears on the report, use date of publication.

7a. TOTAL NUMBER OF PAGES: The total page count should follow normal pagination procedures, i.e., enter the number of pages containing information.

7b. NUMBER OF REFERENCES: Enter the total number of references cited in the report.

8a. CONTRACT OR GRANT NUMBER: If appropriate, enter the applicable number of the contract or grant under which the report was written.

8b, &, & 8d. PROJECT NUMBER: Enter the appropriate military department identification, such as project number, subproject number, system numbers, task number, etc.

9a. ORIGINATOR'S REPORT NUMBER(S): Enter the official report number by which the document will be identified and controlled by the originating activity. This number must be unique to this report.

9b. OTHER REPORT NUMBER(S): If the report has been assigned any other report numbers *(either by the originator or by the sponsor)*, also enter this number(s).

10. AVAILABILITY/LIMITATION NOTICES: Enter any limitations on further dissemination of the report, other than those imposed by security classification, using standard statements such as:

(1) "Qualified requesters may obtain copies of this report from DDC."

(2) "Foreign announcement and dissemination of this report by DDC is not authorized."

(3) "U. S. Government agencies may obtain copies of this report directly from DDC. Other qualified DDC users shall request through _____."

(4) "U. S. military agencies may obtain copies of this report directly from DDC. Other qualified users shall request through _____."

(5) "All distribution of this report is controlled. Qualified DDC users shall request through _____."

If the report has been furnished to the Office of Technical Services, Department of Commerce, for sale to the public, indicate this fact and enter the price, if known.

11. SUPPLEMENTARY NOTES: Use for additional explanatory notes.

12. SPONSORING MILITARY ACTIVITY: Enter the name of the departmental project office or laboratory sponsoring *(paying for)* the research and development. Include address.

13. ABSTRACT: Enter an abstract giving a brief and factual summary of the document indicative of the report, even though it may also appear elsewhere in the body of the technical report. If additional space is required, a continuation sheet shall be attached.

It is highly desirable that the abstract of classified reports be unclassified. Each paragraph of the abstract shall end with an indication of the military security classification of the information in the paragraph, represented as (TS), (S), (C), or (U).

There is no limitation on the length of the abstract. However, the suggested length is from 150 to 225 words.

14. KEY WORDS: Key words are technically meaningful terms or short phrases that characterize a report and may be used as index entries for cataloging the report. Key words must be selected so that no security classification is required. Identifiers, such as equipment model designation, trade name, military project code name, geographic location, may be used as key words but will be followed by an indication of technical context. The assignment of links, rules, and weights is optional.